Ligand binding and activation of UTP-activated G protein-coupled P2Y2 and P2Y4 receptors elucidated by mutagenesis, pharmacological and computational studies

Isaac Y. Attah, Alexander Neumann, Haneen Al-Hroub, Muhammad Rafehi, Younis Baqi, Vigneshwaran Namasivayam, Christa E. Müller

Angaben zur Veröffentlichung / Publication details:

Attah, Isaac Y., Alexander Neumann, Haneen Al-Hroub, Muhammad Rafehi, Younis Baqi, Vigneshwaran Namasivayam, and Christa E. Müller. 2020. "Ligand binding and activation of UTP-activated G protein-coupled P2Y2 and P2Y4 receptors elucidated by mutagenesis, pharmacological and computational studies." *Biochimica et Biophysica Acta (BBA) - General Subjects* 1864 (3): 129501. https://doi.org/10.1016/j.bbagen.2019.129501.

Ligand binding and activation of UTP-activated G protein-coupled $P2Y_2$ and $P2Y_4$ receptors elucidated by mutagenesis, pharmacological and computational studies

Isaac Y. Attah[a,1,2], Alexander Neumann[a,2], Haneen Al-Hroub[a], Muhammad Rafehi[a], Younis Baqi[a,b], Vigneshwaran Namasivayam[a], Christa E. Müller[a,*]

[a] *PharmaCenter Bonn, Pharmaceutical Institute, Pharmaceutical Sciences Bonn (PSB), Pharmaceutical & Medicinal Chemistry, University of Bonn, Germany*
[b] *Department of Chemistry, Faculty of Science, Sultan Qaboos University, PO Box 36, Postal Code 123 Muscat, Oman*

1. Introduction

P2Y receptors (P2YRs) are G protein-coupled receptors (GPCRs) activated by adenine and/or uracil nucleotides. Eight different P2YR subtypes exist which are sub-grouped into $P2Y_1$-like ($P2Y_1$, $P2Y_2$, $P2Y_4$, $P2Y_6$, and $P2Y_{11}$) and $P2Y_{12}$-like ($P2Y_{12}$, $P2Y_{13}$, and $P2Y_{14}$) receptors [1,2]. The $P2Y_1$, $P2Y_{12}$, and $P2Y_{13}$Rs are activated by ADP, $P2Y_2$R is activated by both ATP and UTP, $P2Y_4$R by UTP, $P2Y_6$R by UDP, and $P2Y_{14}$R by both UDP and UDP-glucose [3]. The $P2Y_1$, $P2Y_2$, $P2Y_4$, and $P2Y_6$Rs couple to G_q proteins, $P2Y_{11}$ couples to both G_q and G_s proteins, while the $P2Y_{12}$-like receptor subtypes couple to $G_{i/o}$ proteins. Upon receptor activation by an agonist, G_q proteins stimulate the release of intracellular calcium through the phospholipase C pathway, while G_s and G_i proteins lead to the activation and inhibition of adenylyl cyclase, respectively, thereby modulating intracellular cAMP levels.

P2YRs are widely distributed in the human body and represent

Abbreviations: 2-MeSADP, 2-methylthioadenosine-5′-O-diphosphate; 2-MeSATP, 2-methylthioadenosine-5′-O-triphosphate; ABTS, 2,2′-azino-bis-3-ethylbenzothiazoline-6-sulfonic acid; AP_4A, diadenosine tetraphosphate; AQ, anthraquinone; AR-C118925, 5-{[5-(2,8-dimethyl-5*H*-dibenzo[*a,d*]cyclohepten-5-yl)-3,4-dihydro-2-oxo-4-thioxo-1(2*H*)-pyrimidinyl]methyl}-N-(1*H*-tetrazol-5-yl)-2-furancarboxamide; BSA, bovine serum albumin; DMEM, Dulbecco's Modified Eagle's Medium; DMSO, dimethyl sulfoxide; ECL, extracellular loop; EDTA, ethylenediaminetetraacetic acid; ELISA, enzyme-linked immunosorbent assay; FBS, fetal bovine serum; fluo-4 AM, fluo-4 acetoxymethyl ester; GPCR, G protein-coupled receptor; HA, hemagglutinin; HBSS, Hank's balanced salt solution; *h*$P2Y_2$R, human $P2Y_2$ receptor; *h*$P2Y_4$R, human $P2Y_4$ receptor; *h*$P2Y_x$R, human $P2Y_x$ receptor; IFD, induced fit docking; MRS4062, (((2*R*,3*S*,4*R*,5*R*)-3,4-dihydroxy-5-((*Z*)-2-oxo-4-((3-phenylpropoxy)imino)-3,4-dihydropyrimidin-1-(2*H*)-yl)tetrahydrofuran-2-yl)methyl)triphosphoric acid; PBS, phosphate-buffered saline; RB-2, Reactive blue 2; TM, transmembrane

* Corresponding author at: Pharmazeutisches Institut, Pharmazeutische Chemie I, An der Immenburg 4, D-53121 Bonn, Germany.
E-mail address: christa.mueller@uni-bonn.de (C.E. Müller).
[1] Present address: Department of Biomedical Sciences, School of Health and Allied Sciences, University of Cape Coast, Cape Coast, Ghana.
[2] Equal contribution.

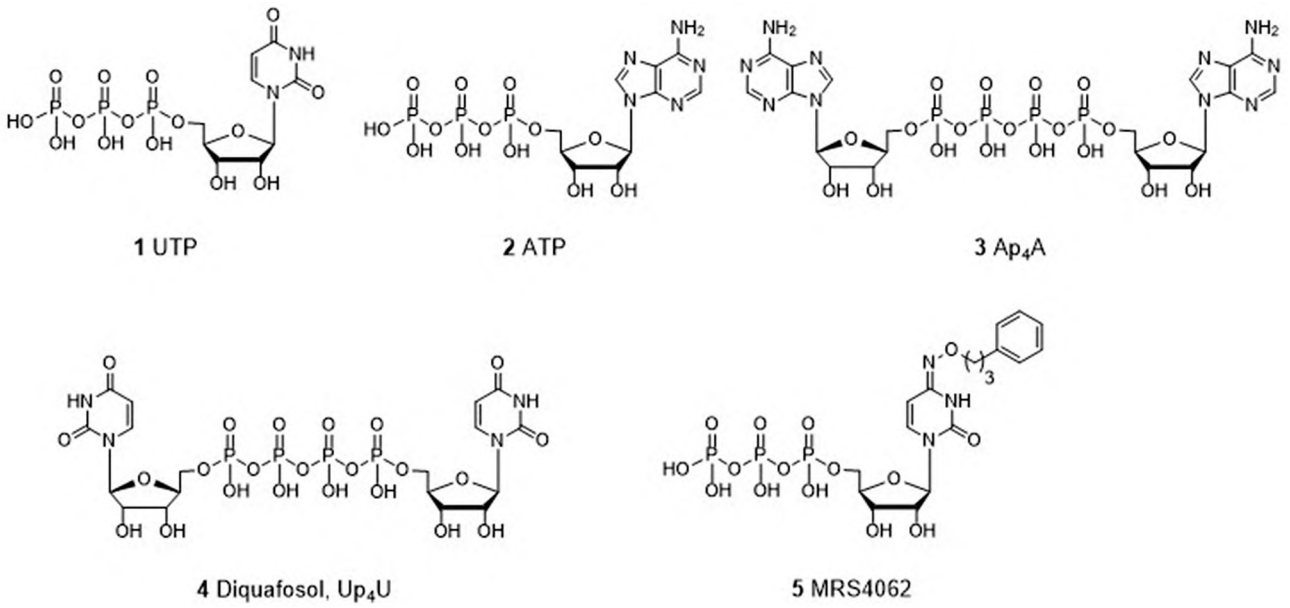

Fig. 1. Structures of selected P2Y receptor agonists.

(potential) therapeutic targets for several diseases including thrombosis, inflammation, neurodegenerative diseases and cancer [4,5]. For instance, several antagonists of the ADP-activated $P2Y_{12}R$ are marketed as antithrombotic drugs, namely clopidogrel, prasugrel, cangrelor and ticagrelor [6–8]. However, at present there are no drugs available for the uracil-activated $P2Y_4$, $P2Y_6$ and $P2Y_{14}$ receptors and only one (diquasofol) for the $P2Y_2R$ [9–11]. In the present study, we focused on the closely related $P2Y_2$ and $P2Y_4$ receptor subtypes.

The $P2Y_2R$ is the only member of the P2Y receptor family that is activated by both UTP (**1**) and ATP (**2**) (see Fig. 1) with comparable potencies and efficacies [2,12]. It is additionally activated by dinucleotides such as Ap_4A (**3**) [13]. $P2Y_2R$ is widely expressed in the body, e.g. in brain, lungs, heart, liver, stomach, skeletal muscle, spleen and bone marrow [14–16]. Agonists of the $P2Y_2R$ have been proposed for the treatment of cystic fibrosis, chronic bronchitis, viral infections, myocardial infarction and Alzheimer's disease (AD) [17]. Diquafosol (Up_4A, **4**), a $P2Y_2R$ agonist, is in fact used for treating dry eye disease in Asia [18–22]. In AD, activation of $P2Y_2R$ expressed in microglia mediates phagocytosis and degradation of the insoluble fibrillar β-amyloid and oligomeric β-amyloid aggregates that are neurotoxic [23]. Moreover, activation of the $P2Y_2R$ mediates an increase in α-secretase-dependent non-amyloidogenic cleavage of the amyloid precursor protein (APP). $P2Y_2R$ agonists have also been reported to be cardio-protective during hypoxia and myocardial infarction in cultured rat cardiomyocytes and *in vivo* in mice [24,25].

Antagonists of the $P2Y_2R$, on the other hand, may be useful as drugs for preventing cancer metastasis and for the treatment of obesity, diabetes insipidus and inflammatory conditions including asthma [5,23,26–31]. Only few antagonists have been reported so far that can be utilized as pharmacological tools for studying the $P2Y_2R$. These include the non-selective P2YR antagonist reactive blue 2 (RB-2, **6**) and the selective $P2Y_2R$ antagonist AR-C118925 (**7**) (for structures see Fig. 2) [32–34].

The $P2Y_2R$ is closely related to the $P2Y_4R$. Both receptors share the highest amino acid sequence identity among the human (h) P2YR subtypes (53%), compared to sequence identities of 34% for $P2Y_2$/$P2Y_1$, 38% for $P2Y_2$/$P2Y_6$ and 21% for $P2Y_2$/$P2Y_{12}$.

The $P2Y_4R$ is widely distributed in the body, including brain, lung and intestine. It regulates chloride secretion in the jejenum. In the brain, it is involved in regulating the production and secretion of amyloid precursor proteins [35–38]. Agonists for the $P2Y_4R$ are therefore, like those for the $P2Y_2R$, of interest as drugs for the treatment of cystic fibrosis [39] and AD [3]. In AD, activation of microglial $P2Y_4Rs$ leads to pinocytosis of soluble $A\beta_{1-42}$ from the neuronal extracellular environment and thus prevents Aβ accumulation which would eventually result in synaptic dysfunction [23,40]. Antagonists of the $P2Y_4R$ might be used for the treatment of diarrhea caused by bacterial infections [39] and for the treatment of diabetic neuropathy [41]. $P2Y_4R$ antagonists have also been reported to be protective in early stage of myocardial infarct [42,43].

The human $P2Y_4R$ (*h*$P2Y_4R$) is activated by UTP (**1**) and blocked by ATP (**2**) and Ap_4A (**3**). In contrast, ATP is a full agonist at the rat $P2Y_4R$. MRS4062 (**5**), an N^4-phenylpropoxy-substituted cytidine-5′-triphosphate derivative, was reported to be a selective agonist of *h*$P2Y_4R$ (EC_{50} = 0.023 μM) with 28- and 38-fold selectivity over $P2Y_2R$ and $P2Y_6R$, respectively [44]. Few antagonists have been described for the $P2Y_4R$ so far. Those commonly used as pharmacological tools include the non-selective P2YR antagonist RB-2 (**6**) and pyridoxalphosphate-6-azophenyl-2′,4′-disulfonic acid (PPADS, **8**) [45,46]. Recently, the anthraquinone (AQ) derivatives PSB-09114 (**9**), PSB-16133 (**10**), PSB-16135 (**11**), and PSB-1699 (**12**) have been reported as antagonists of the $P2Y_4R$ displaying moderate potency and selectivity [47].

Despite their therapeutic potential, selective, orally bioavailable agonists and antagonists for $P2Y_2$- and $P2Y_4Rs$ are hardly available. In order to be able to design ligands, knowledge of the topography of the binding site(s) of these receptors is required. To this end, we employed molecular modeling and site-directed mutagenesis studies. While the X-ray crystallographic structures of the $P2Y_2$- and $P2Y_4Rs$ are not available, those of the P2YR subtypes $P2Y_1$ and $P2Y_{12}$ have been published, which can serve as templates for homology modeling [48,49]. Recently, our group published a $P2Y_2R$ homology model based on the crystal structures of *h*$P2Y_1R$. Preliminary data from site-directed mutagenesis studies in combination with docking studies for UTP, Ap_4A and AR-C118925 using that model shed light on key interactions with amino acids in the orthosteric binding pocket of the $P2Y_2R$ structure [50]. The docking results suggested a binding mode for agonists similar to that of 2Me-SADP and 2Me-SATP in *h*$P2Y_{12}R$ [2], which differs from the binding mode of the nucleotide antagonist MRS2500 (**13**) in complex with *h*$P2Y_1R$ [49]. Moreover, we published a homology model of *h*$P2Y_4R$ and used it to predict the binding site of AQ antagonists [47].

In the present study, we performed site-directed mutagenesis to specifically address the question, how selective ligand binding at the

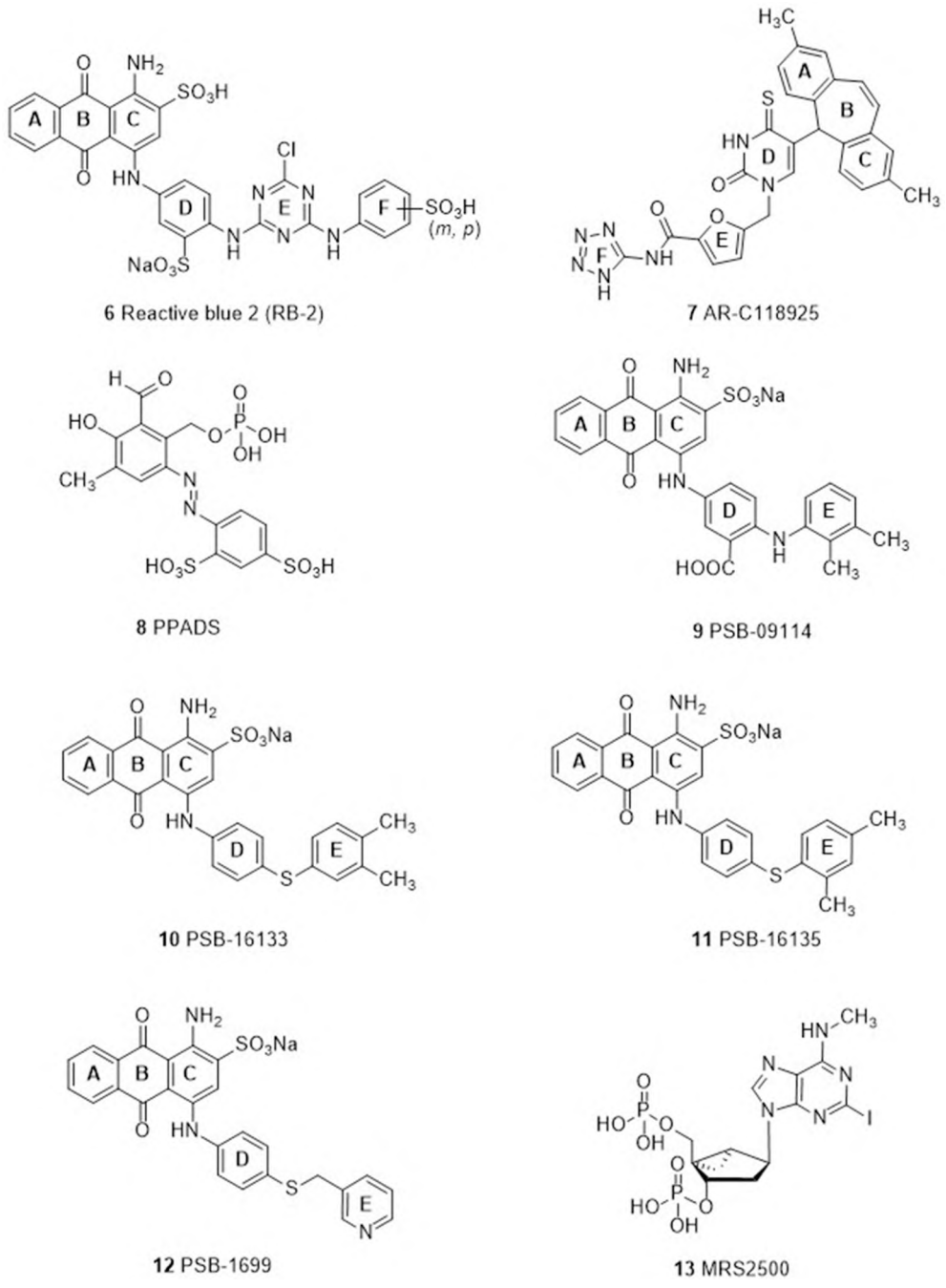

Fig. 2. Structures of selected P2YR antagonists.

closely related P2Y receptor subtypes $P2Y_2$ and $P2Y_4$ can be achieved. We investigated agonist binding modes, and agonist discrimination, e.g. ATP versus UTP, as well as binding modes of antagonists.

2. Materials and methods

2.1. Materials

The restriction enzymes and T4 DNA ligase were obtained from New England BioLabs (Frankfurt am Main, Germany) while the DNA polymerase Pyrobest was purchased from TaKaRa Bio Inc. (Saint-Germain-en-Laye, France). All primers used in the current work were synthesized by MWG Biotech (Ebersberg, Germany). The agar for cloning and the chromophore solution 2,2′-azino-bis-3-ethylbenzothiazoline-6-sulfonic acid (ABTS) were purchased from Calbiochem (Darmstadt, Germany). Dulbecco's Modified Eagle Medium (DMEM), penicillin/streptomycin, trypsin-EDTA (ethylenediaminetetraacetic acid), and lipofectamine 2000 were obtained from Life Technologies GmbH (Darmstadt, Germany). Fluo-4 acetoxymethyl ester (Fluo-4-AM) was obtained from Invitrogen/Thermo Fisher (Merelbeke, Belgium) while geniticin (G418) was from PAN Biotech (Aidenbach, Germany). Fetal bovine serum (FBS) was purchased from Sigma–Aldrich (Taufkirchen, Germany). The hemagglutinin-(HA)-specific mouse monoclonal antibody (HA.11) was obtained from Covance, Berkeley, CA, USA. Ap_4A was and UTP were bought from Sigma–Aldrich (Steinheim, Germany) and ATP from ROTH, Carl Roth GmbH (Karlsruhe, Germany). MRS4062 was bought from Tocris Bioscience (Bristol, UK) and carbachol from Alfa Aesar Thermo Fisher GmbH (Kandel, Germany). Corning 3340 microplates were purchased from Corning Life Sciences (Tewksbury, Massachusetts, USA), and 24-well plates for ELISA assays from Sarstedt AG & Co. (Nuembrecht, Germany).

2.2. Homology modeling

Previously, we reported on homology models for *h*P2Y$_2$- and *h*P2Y$_4$Rs [47,50]. Both had been based on the X-ray crystal structure of *h*P2Y$_1$R in complex with the nucleotide antagonist MRS2500 (PDB-ID: 4XNW). These were used as starting points in the present study [49].

2.3. Docking studies

The previously published procedure was used for docking studies with the Induced Fit Docking and Glide Docking modules implemented in the Schrödinger software package release 2016 [51]. To limit docking to the putative orthosteric binding site, the aspartic acid residues Asp185^{ECL2} (P2Y$_2$R) and Asp187^{ECL2} (P2Y$_4$R), residues assumed to be involved in receptor activation as discussed below, were selected as the receptor center. The putative orthosteric binding site was derived from the X-ray crystal structure of *h*P2Y$_{12}$R in complex with the orthosteric agonists 2-methylthio-ADP (2MeSADP) and 2-methylthio-ATP (2MeSATP) (PDB-IDs: 4PXZ, 4PY0) [52]. Ligands were docked into a box with a side length of 25.0 Å around the aspartic acid residue Asp185^{ECL2} (P2Y$_2$R) and Asp187^{ECL2} (P2Y$_4$R). The best docking pose was selected based on the induced fit docking (IFD) score and Prime Energy values.

In the case of the agonist MRS4062 (**5**) no conclusive docking position in the P2Y$_4$R was achievable due to steric hindrance by Tyr116$^{3.33}$. Therefore, we introduced a computational Y116$^{3.33}$A mutant to increase the space of the binding cavity, and docked MRS4062 using the published procedure. The best docking pose was selected, and the Y116$^{3.33}$A mutation was subsequently reverted. The Tyr116$^{3.33}$ rotamer with the lowest energy value was selected for the final docking pose.

During docking of the AQ-derived antagonists, the highest-ranked protein complex of P2Y$_2$R with PSB-16133 (**10**) was considered as a template for further dockings, since we expected the ligands to have a similar binding mode with respect to the induced rotamers. The ligands were subsequently redocked with the most reasonable docking pose using extra precision (XP) glide docking. The top scoring docking poses were evaluated with their scores and Prime Energy.

2.4. Site-directed mutagenesis studies

The sequences of *h*P2Y$_2$(ID P41231) and *h*P2Y$_4$Rs (ID P51582) used for site-directed mutagenesis studies were taken from the Uniprot database [53]. Whole plasmid recombinant polymerase chain reaction (PCR) using the appropriate primers was performed using the puc19 vector to introduce the desired point mutations. PCR was performed as follows: 30 s at 98 °C, 30 cycles, each consisting of 10 s at 98 °C, 40 s at the appropriate annealing temperatures (°C), and 5 min of primer extension at 72 °C. The PCR products were treated with *Dpn*I to digest the template plasmid, then purified and used to transform competent *E. coli* bacteria. For each receptor, wildtype (wt) or mutant, cDNA was isolated from individual clones and recombinantly cloned into the mammalian retroviral vector pLXSN with the influenza hemagglutinin (HA) epitope attached to the N-terminus. All DNA sequencing data were generated by GATC Biotech (Cologne, Germany), confirming the expected sequences.

2.5. Retroviral transfection

One day before transfection, 1.5 × 10^6 GP + envAM12 packaging cells were seeded into a small 25 cm^2 cell culture flask with Dulbecco's Modified Eagle's Medium (DMEM) medium supplemented with 10% FBS and 100 U/mL penicillin G and 100 µg/mL streptomycin. A few hours before the transfection, the medium was changed to 6.25 µL of DMEM medium containing only 10% FBS. Transfection involved the delivery of a total of 10 µg DNA - 6.25 µg of receptor-containing plasmid-DNA and 3.75 µg of the vesicular stomatitis virus G protein (VSV-G) - into the packaging cells using Lipofectamine 2000. After incubating the transfected cells at 37 °C for 12–15 h, the medium was changed to 3 mL DMEM supplemented with 10% FBS, 100 U/mL penicillin G, 100 µg/mL streptomycin and 5 mM of a sterile aqueous solution of sodium butyrate. The cells were then incubated at 32 °C with 5% CO_2 for 48 h. About 24 h before infection, 5 × 10^5 1321 N1 astrocytoma cells were seeded into a 25 cm^2 flask containing DMEM medium with 10% FBS, 100 U/mL penicillin G and 100 µg/mL streptomycin, and incubated at 37 °C. On the day of infection, the medium was removed from the astrocytoma cells and discarded. The medium (containing viruses) was removed from the GP + envAM12 cells, filtered through a 0.22 µm filter onto the astrocytoma cells followed by 6 µL of sterilized polybrene solution (4 mg/mL in water). The astrocytoma cells were then incubated at 37 °C for 2½ h after which the medium was exchanged for 5 mL of DMEM medium containing 10% FBS, 100 U/mL penicillin G and 100 µg/mL streptomycin. The medium was replaced after 48 h of incubation by DMEM with 10% FBS, 100 U/mL penicillin G, 100 µg/mL streptomycin and 800 µg/mL G418 for selection of cells expressing the receptor.

2.6. Cell culture

The 1321 N1 astrocytoma cells were cultured in DMEM supplemented with 1% ultraglutamine, 10% FBS, 100 U/mL penicillin G, and 100 µg/mL streptomycin. They were stably transfected with either the wt or mutant P2Y$_2$ or P2Y$_4$R. The DMEM medium described above was further supplemented with 800 µg/mL G418. The GP + envAM12 packaging cells were maintained in HXM (hypoxanthine, xanthine, mycophenolic acid) media containing DMEM supplemented with 1% ultraglutamine, 10% FBS, 100 U/mL penicillin G, 100 µg/mL streptomycin, 15 µg/mL hypoxanthine, 250 µg/mL xanthine, 25 µg/mL mycophenolic acid, and 200 µg/mL hygromycin B. All cells were grown at 37 °C in 96% humidified air.

2.7. Cell surface enzyme-linked immunosorbent assay (ELISA)

The 1321 N1 astrocytoma cell-line expressing the various wt or mutant receptors were seeded in duplicates at a density of 150,000 cells per well into a 12-well plate 24 h before the assay. The medium was removed and the cells were washed with phosphate-buffered saline (PBS). 500 µL of 1% bovine serum albumin (BSA) in PBS was added for 5 min to block non-specific cell surface binding. Next, 300 µL of a 1:1000 dilution of the hemagglutinin (HA)-specific mouse monoclonal antibody (HA.11) solution in DMEM containing 1% BSA was added to each well and the mixture was incubated at room temperature (rt) for 1 h. The cells were washed three times with 500 µL of PBS, fixed with 500 µL of 4% paraformaldehyde in PBS, pH 7.3, washed again with 500 µL of PBS and blocked with 500 µL of 1% BSA in PBS for 10 min. The cells were then incubated at rt. for 1 h with 300 µL of peroxidase-conjugated goat anti-mouse IgG antibody of a 1:2500 dilution ratio in DMEM supplemented with 1% BSA. After further washing with 500 µL PBS for four times, the cells were incubated with 300 µl of the substrate, ABTS solution, for 45 min at rt. Finally, 170 µL aliquots of the supernatant ABTS solution were then transferred into a 96-well plate, and the absorbance was measured at 405 nm by a PHERAstar microplate reader (BMG Laboratory Technologies, Offenburg, Germany). The whole assay, except for the addition of antibodies and the substrate reaction, was performed on ice and with freshly prepared cold buffers.

2.8. Calcium mobilization assay

About 16–24 h before the assay, the growth medium was removed from a T175 mL flask with approximately 80–90% cell confluency. The cells were washed with PBS (containing 137 mM NaCl, 2.7 mM KCl, 4.3 mM Na_2HPO_4, and 1.47 mM KH_2PO_4, at pH 7.3). Then, they were detached with trypsin-EDTA and re-suspended in supplemented DMEM (see above). To each well of the sterile black 96-well polystyrene plate with a transparent flat bottom (Corning 3340), about 60,000 cells in 200 µL DMEM growth medium were added and subsequently incubated at 37 °C, 96% humidity and 10% CO_2. Prior to the assay, the growth medium was removed completely and the adherent cells were incubated

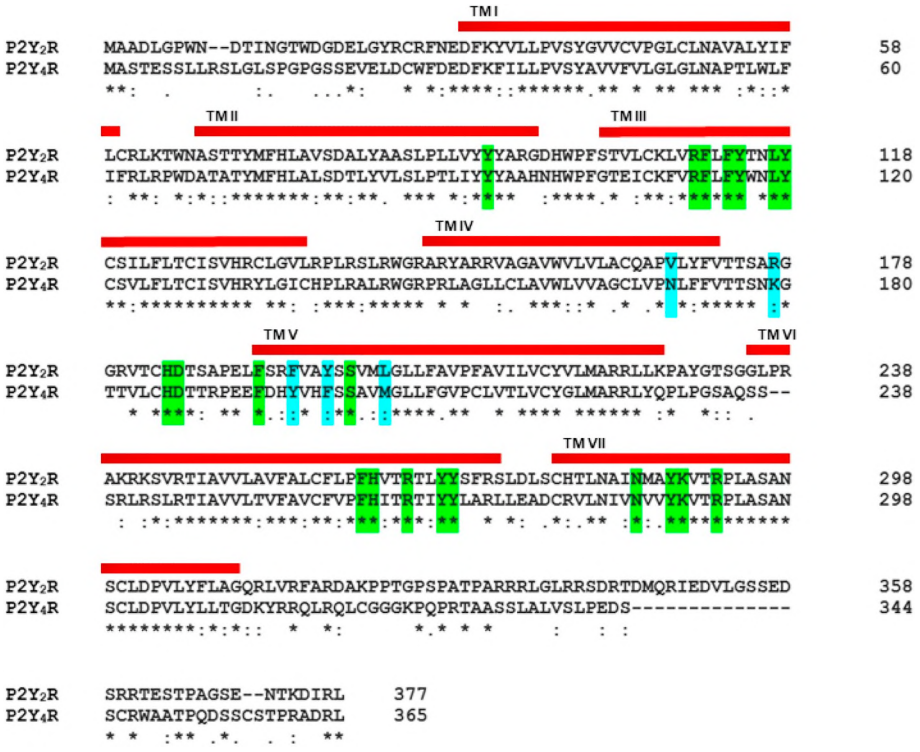

Fig. 3. Sequence alignment of *h*P2Y$_2$- and *h*P2Y$_4$Rs. Transmembrane regions (denoted as 'TM') are indicated by red bars. Identical residues of the putative orthosteric binding site are highlighted in green, non-identical residues are highlighted in blue.

with 40 µL of loading dye, consisting of 15 µL of fluo-4 acetoxymethyl ester (1 mM solution in dimethyl sulfoxide (DMSO)) and 15 µL Pluronic F-127 (25% *w/v* in DMSO) in 4970 µL Hank's balanced salt solution (HBSS) buffer, in each well, for 1 h. After incubation, the excess dye was removed, and cells were further incubated in HBSS buffer at rt for 30 min before the addition of agonists. For assessment of antagonist potencies, the cells were pre-incubated with the antagonists in HBSS buffer during the 30 min incubation before addition of the agonist at its EC_{80} concentration. All dilutions used for concentration–response curves were performed on a log-scale. The final volume in each well was 200 µL, and the final DMSO concentration was 0.5%. The measurement of fluorescence intensities was performed on a Novostar plate reader (BMG LabTechnologies, Offenburg, Germany) at 520 nm for 30 s at 0.4 s intervals after excitation at 485 nm. For all assays, 100 µM carbachol, inducing intracellular Ca^{2+} release by activating the natively expressed G_q protein-coupled muscarinic M_3 receptor (M_3R) in 1321 N1 astrocytoma cells, was used as a positive control. The maximal carbachol response was set at 100% and employed for normalization of all other responses.

3. Results and discussions

3.1. Molecular modeling

Sequence alignment as well as previously published homology models of the *h*P2Y$_2$R and the *h*P2Y$_4$R were employed to predict residues of interest that were selected for site-directed mutagenesis studies [47,50]. While several mutagenesis studies of human and rat P2Y$_2$Rs have been reported, only limited data is available for P2Y$_4$R [12,50,54]. A comparative study between N-terminus and extracellular loop 2 (ECL2) of the *h*P2Y$_4$R (activated by UTP) and the rat P2Y$_4$R (activated by both UTP and ATP) was previously performed by studying chimeric receptors [55]. Ten chimeras of the *h*P2Y$_4$R, in which the extra- and intracellular regions were exchanged for those of the rat P2Y$_4$R, had been constructed. The amino acid residues Asn177^{ECL2}, Ile183 ^{ECL2}, and Leu190^{ECL2} were reported to contribute to the acceptance of ATP as an agonist by the *h*P2Y$_4$R chimera, in which the ECL2 was exchanged for that of the rat P2Y$_4$R.

Although *h*P2Y$_2$- and *h*P2Y$_4$Rs share only a moderate sequence identity (53%), the predicted orthosteric binding pocket is rather conserved, except for three residues (see Fig. 3): Tyr197$^{5.35}$ of P2Y$_4$R is replaced by phenylalanine in P2Y$_2$R, Val204$^{5.42}$ is replaced by methionine, and Met205$^{5.43}$ by leucine. Tyr197$^{5.35}$ is conserved in the human, rat and mouse P2Y$_4$R, while the corresponding phenylalanine is conserved in the human, rat, and mouse P2Y$_2$R (see Fig. S1 in Supplementary Information). Val204$^{5.42}$ is not highly conserved, as it is exchanged for isoleucine in the mouse P2Y$_4$R. Met205$^{5.43}$, on the other hand, is conserved in P2Y$_4$R of all three species. This leads to the conclusion that either a single or multiple mutations or other contributors like the ECL2 itself may be responsible for agonist discrimination.

3.1.1. Docking studies at the P2Y$_2$R

We previously reported on the binding mode of UTP in *h*P2Y$_4$R based on a homology model [50]. The endogenous agonist UTP is proposed to bind in the upper third part of the receptor in a cleft formed by side-chains of TM III, VI and VII, as it is common for many GPCRs (see Fig. 4) [49,56]. The phosphate groups are proposed to interact with positively charged amino acid residues (arginine, lysine, histidine). The nucleobase likely binds in a lipophilic binding cavity formed by phenylalanine and tyrosine residues. Docking studies of UTP into the homology model of *h*P2Y$_2$R propose a similar binding mode. For detailed discussion of interactions see below (Section 3.5.1).

Based on previously published docking studies of the agonist UTP into the homology model of *h*P2Y$_2$R, and the predicted binding mode of UTP in the homology model of *h*P2Y$_4$R, we selected 14 amino acid residues (five of P2Y$_2$R and nine of P2Y$_4$R) for site-directed mutagenesis.

3.1.1.1. P2Y$_2$R. Molecular dynamics simulation studies suggested an ionic lock between an aspartic acid residue in the extracellular loop 2 (ECL2) and an arginine in TM VII to play a key role in P2Y$_1$R activation; agonists were proposed to break the ionic lock between Asp204^{ECL2} and Arg310$^{7.39}$, while antagonists were predicted to stabilize the interaction

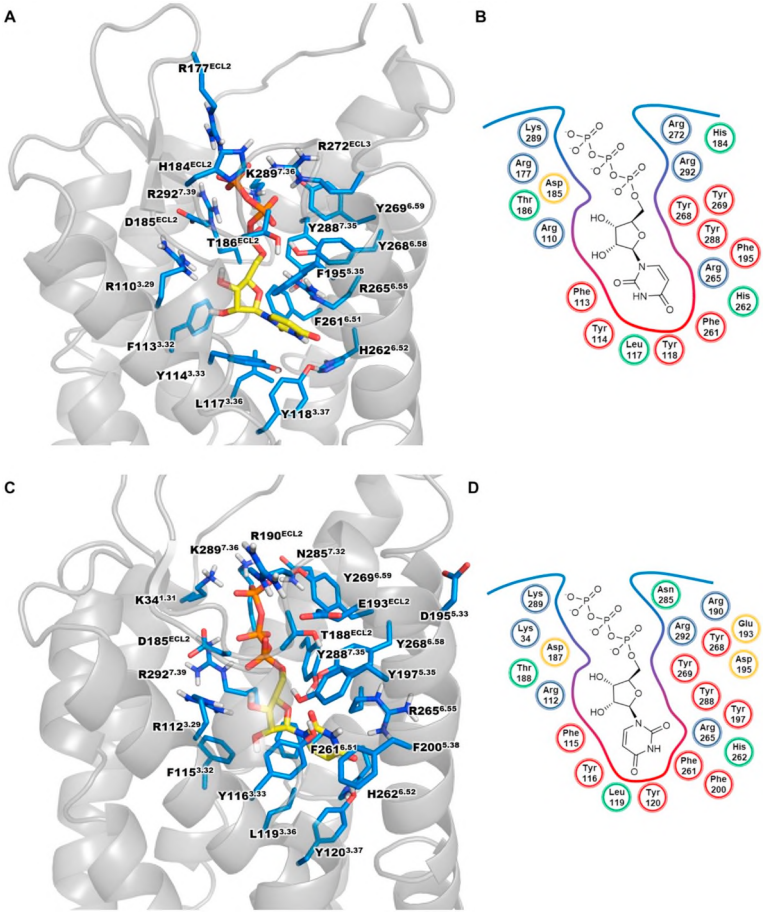

Fig. 4. Putative binding mode of UTP in the homology models of *h*P2Y$_2$- (**A** and **B**) and *h*P2Y$_4$Rs (**C** and **D**). **A**. Docked pose of UTP with the important residues in the binding pocket is shown. **B**. Schematic 2D representation of the binding pocket. **C**. Docked pose of UTP in *h*P2Y$_4$R homology model. **D**. Schematic 2D representation of the UTP-P2Y$_4$R complex. P2Y$_2$- and P2Y$_4$Rs (gray) are displayed in cartoon representation, the amino acid residues (blue) and UTP (yellow) are shown as stick models; oxygen atoms are colored in red, nitrogen atoms in blue, phosphorus atoms in orange (**A**, **C**). Charged, basic residues are colored in blue, aromatic residues in red, the conserved aspartic acid residue in the ECL2 involved in an ionic lock with Arg292$^{7.39}$ is depicted in yellow, other residues in the binding pocket in green (**B**, **D**).

thereby preventing receptor activation [57]. Mutagenesis studies on *h*P2Y$_1$R had shown that both residues play key roles in agonist-induced receptor activation [58]. In our previous studies we were able to confirm P2Y$_2$-Arg292$^{7.39}$ as an important residue for agonist function, which is the analogous residue to P2Y$_1$-Arg310$^{7.39}$. To further investigate the role of an ionic lock between ECL2 and TM VII in P2Y$_2$R, we selected the P2Y$_2$-D185^{ECL2}A mutant. P2Y$_2$-R110$^{3.29}$A, a previously published mutant [50] was additionally investigated in this study for possible consequences on P2Y$_2$R interaction with the recently published agonist MRS4062 [44]. P2Y$_2$-Phe113$^{3.32}$ is predicted to be part of the orthosteric binding site of P2Y$_2$R. Therefore, it was mutated to alanine and tyrosine, respectively, to investigate its interactions with the nucleobases of the agonists. P2Y$_2$-Phe195$^{5.35}$, corresponding to Tyr197$^{5.35}$ in *h*P2Y$_4$R, is located close to the ECL2 in the upper part of TM V. These represent non-conserved residues in the predicted orthosteric binding pocket of P2Y$_2$- and P2Y$_4$Rs, which might play a role in the acceptance of UTP versus ATP.

3.1.1.2. P2Y$_4$R. For mutation of *h*P2Y$_4$R, Asn170$^{4.60}$ was selected as it is close to the putative orthosteric binding site and replaced by Val168$^{4.60}$ in P2Y$_2$R. Arg194^{ECL2} was found to play a role in ligand recognition by P2Y$_2$R even though it is distant from the putative orthosteric binding site [50]. It was concluded, that Arg194^{ECL2} may form a salt bridge with Glu190^{ECL2} forming a second ionic lock close to the TMV and ECL2, that modifies the flexibility of the loop, resulting in decreased potency of agonists. Therefore, we decided to investigate Arg190^{ECL2}, Glu193^{ECL2} and Asp195$^{5.33}$ in P2Y$_4$R as those amino acid residues may form an analogous ionic lock in P2Y$_4$R. Finally, Tyr197$^{5.35}$ and Phe200$^{5.38}$ of P2Y$_4$R were selected as candidates for mutagenesis studies, as they are close to the putative orthosteric binding site and not conserved between the two related P2YR subtypes.

All mutants selected for mutagenesis in the present study are presented in Fig. 5. New and published mutagenesis data for P2Y$_2$- and P2Y$_4$Rs were taken into account for the analysis and prediction of binding modes of agonists and antagonists. The mutants were recombinantly expressed in 1321 N1 astrocytoma cells, and their effects on selected ligands were investigated by calcium mobilization studies. Four agonists, UTP (**1**), ATP (**2**), Ap$_4$A (**3**), and MRS4062 (**5**) were evaluated. The investigated antagonists included AR-C118925 (**7**), and the AQ derivatives RB-2 (**6**), PSB-09114 (**9**), PSB-16133 (**10**), PSB-16135 (**11**), and PSB-1699 (**12**). The ligand selection was based on structural diversity, differences in size, and unique pharmacological profiles, i.e. selectivity for either receptor subtype.

3.2. Site-directed mutagenesis studies

The coding sequences of P2Y$_2$- and the P2Y$_4$Rs were cloned into the plasmid vector pUC19, and using whole plasmid PCR, the desired point mutations were introduced. From pUC19, the cDNAs were cloned into the pLXSN retroviral expression vector featuring a hemagglutinin (HA) epitope sequence at the N-terminus of the receptors. The wt and mutant receptors were then stably transfected into 1321 N1 astrocytoma cells. Since expression levels can directly affect the potency of GPCR agonists in functional assays [59,60], these were determined by enzyme-linked immunosorbent assay (ELISA) using an antibody against the HA-tag. Previous reports had shown that the HA-tag does not interfere with ligand–receptor pharmacology [12,50]. All data were normalized to the expression of the wt receptor (see Fig. 6 and Appendix Table S1 for expression values). Cell surface expression of the P2Y$_2$R mutants was between 16% and 125% relative to that of the wt receptor (100%). The receptor with the lowest expression was the P2Y$_2$R-F113$^{3.32}$Y mutant (16 ± 1%), which is a highly conserved amino acid among the two investigated P2YR subtypes (see Fig. 6). In contrast to F113$^{3.32}$Y, the P2Y$_2$R-mutant F113$^{3.32}$A showed high expression

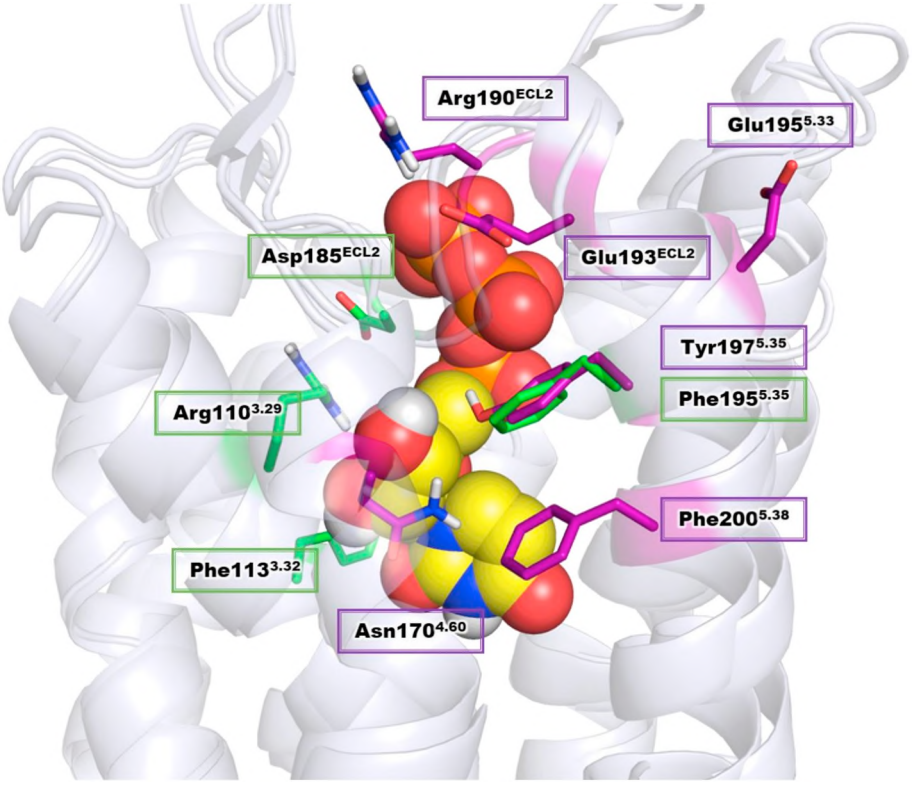

Fig. 5. Putative binding mode of UTP in the homology model of *h*P2Y$_2$R in overlay with the homology model of *h*P2Y$_4$R used for selection of amino acid residues for mutagenesis. P2Y$_2$- and the P2Y$_4$R are displayed in cartoon representation, the amino acid residues of P2Y$_2$- (green) and P2Y$_4$Rs (purple) to be mutated are shown as stick models, UTP as spheres. Carbon atoms are colored in yellow, hydrogen atoms in white, oxygen atoms in red, nitrogen atoms in blue, and phosphorus atoms in orange.

(125 ± 10%). P2Y$_2$R-R110$^{3.29}$A mutant displayed a high cell surface expression (74 ± 4%) similar as in a previous study [50]. Cell surface expression of the P2Y$_4$R mutants was between 56 ± 2% (Y197$^{5.35}$A) and 144 ± 6% (F200$^{5.38}$Y) relative to that of the wt P2Y$_4$R (100%).

3.3. Analysis of agonist activities

Four agonists, UTP (**1**), ATP (**2**), Ap$_4$A (**3**) and MRS4062 (**5**), were selected for testing at the receptors based on their structures and their pharmacology. UTP activates both receptor subtypes. ATP and Ap$_4$A only activate P2Y$_2$R while MRS4062 was reported to be selective for P2Y$_4$R. The ligands were assessed by measuring intracellular calcium concentrations using the fluorescent calcium-chelating dye Fluo-4. 1321 N1 Astrocytoma cells natively express the muscarinic M$_3$R which is also G$_q$ protein-coupled and therefore, like the P2Y$_2$- and P2Y$_4$Rs, leads to intracellular calcium release upon activation. Carbachol, a muscarinic M$_3$R agonist was therefore used as an internal standard to which all data were normalized. In addition, data for all agonist efficacies at each mutant were normalized to UTP efficacy at the corresponding wt receptors. Concentration–response curves are shown in Figs. 7, 9 and 10, pEC$_{50}$ values and efficacies are presented in Figs. 8 and 11 while EC$_{50}$ values are collected in Tables S2 and S3 of Supplementary Information.

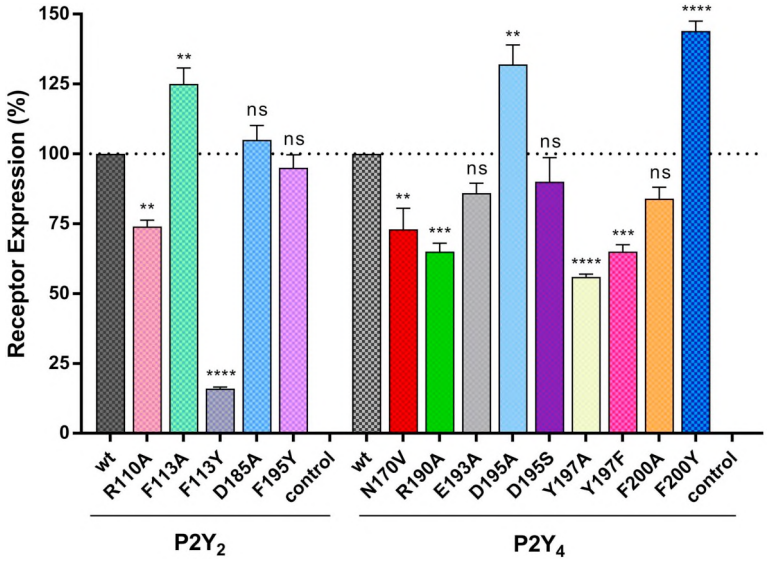

Fig. 6. Cell surface receptor expression levels as determined by ELISA using antibodies interacting with the HA tag fused to the N-terminus of P2Y$_2$- and P2Y$_4$Rs. Data represent means ± SEM of 3–4 independent experiments (in duplicates). Expression rates of the mutants were determined relative to that of the wt (100%). Statistical analysis was done using one-way ANOVA with Dunnett's post-hoc test: ^{ns} not significant; * $p \leq .05$; ** $p \leq .01$; *** $p \leq .001$; **** $p \leq .0001$.

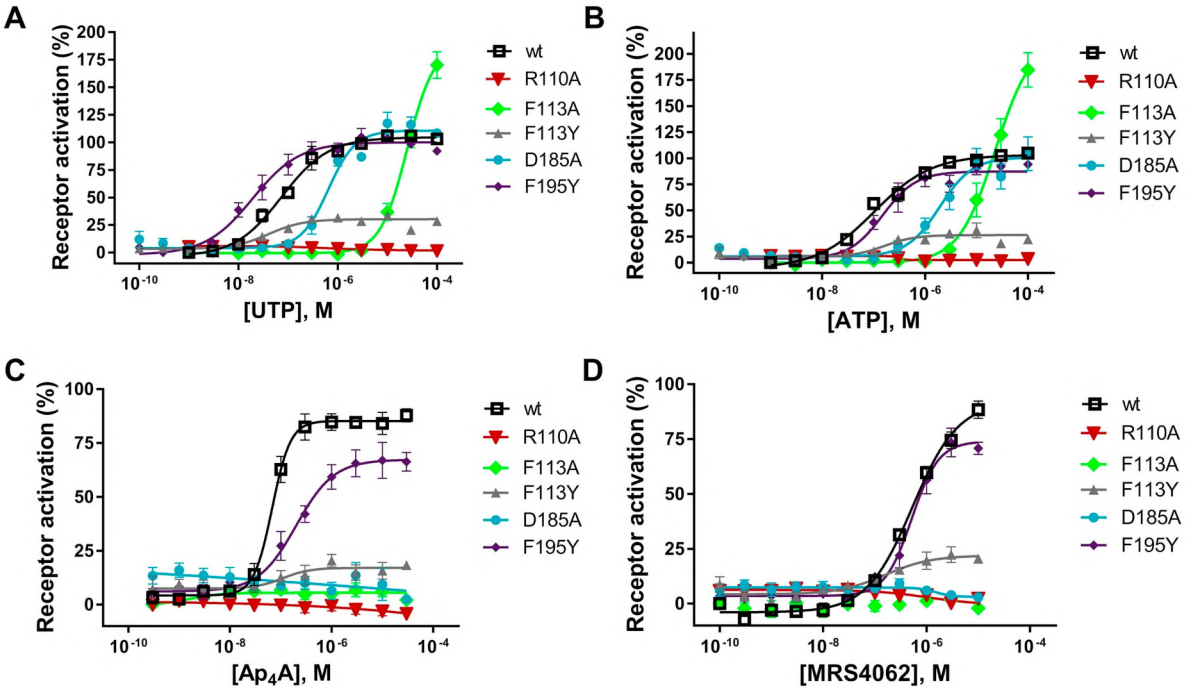

Fig. 7. Concentration–response curves of **(A)** UTP **(B)** ATP **(C)** Ap_4A and **(D)** MRS4062 determined by calcium mobilization assays on the wt and mutant $P2Y_2$Rs expressed in 1321 N1 astrocytoma cells. Each data point represents the mean ± SEM of 4–6 independent determinations each in duplicates. EC_{50} values are reported in Supplementary Information, Table S2.

3.3.1. Evaluation of agonists at the $P2Y_2R$

3.3.1.1. UTP. UTP (**1**) displayed an EC_{50} value of 0.0822 ± 0.0059 μM at *h*$P2Y_2R$, which is consistent with previous reports in calcium assays [12,50]. We observed a rightward shift of the concentration–response curves for most of the mutants relative to the wt receptor, except for the $F195^{5.35}Y$ mutant at which UTP showed an EC_{50} value of 0.0233 ± 0.0064 μM (see Figs. 7 and 8; Table S2). There was no significant difference ($p > .05$) between the potencies at the wt and the $F113^{3.32}Y$ receptor mutant despite its comparatively lower expression level (16% of the wt $P2Y_2R$). The $R110^{3.29}A$ mutation resulted in a complete loss of receptor activation for all four tested agonists. The potency of UTP decreased by 300-fold at the $F113^{3.32}A$ mutant (EC_{50} 25.0 ± 2.7 μM, $p \leq .0001$, ****) whereas at the $D185^{ECL2}A$ mutant it decreased 7-fold compared to that at the wt $P2Y_2R$ (0.606 ± 0.076 μM vs 0.0822 ± 0.0059 μM). There was a 3-fold increase in UTP potency at the $F195^{5.35}Y$ mutant (EC_{50} 0.0233 ± 0.0064 μM, $p \leq .01$, **). The efficacies of UTP at the $P2Y_2$ mutants ranged between 33% and 170% compared to the wt $P2Y_2R$. A significant change in UTP efficacy was observed for the $F113^{3.32}A$ (170 ± 12%, $p \leq .0001$, ****) and the $F113^{3.32}Y$ (33 ± 2%, $p \leq .0001$, ****) mutants compared to the wt receptor (see Fig. 8).

3.3.1.2. ATP. ATP (**2**) was about equipotent to UTP at the wt *h*$P2Y_2R$ (EC_{50} 0.102 ± 0.010 μM) with nearly the same efficacy (see Table S2). Similar to UTP, concentration–response curves were slightly rightward-shifted for ATP at most of the mutants (i.e. $F113^{3.32}A$, $F113^{3.32}Y$, $D185^{ECL2}A$ and $F195^{5.35}Y$), with significant differences in potencies (see Figs. 7 and 8). Like UTP, ATP was completely inactive at the $R110^{3.29}A$ mutant although this mutant was highly expressed. Disruption of the ionic lock in the $D185^{ECL2}A$ mutant led to a 21-fold reduction in ATP potency (EC_{50} 2.160 ± 0.454 μM, $p \leq .0001$, ****) relative to the wt $P2Y_2R$. Also, the receptor mutants $F113^{3.32}A$ and $F113^{3.32}Y$ showed appreciable differences in ATP activity as compared to the wt $P2Y_2R$. At $F113^{3.32}A$, ATP (**2**) was 200-fold less potent (EC_{50} 20.5 ± 4.2 μM, $p \leq .0001$, ****) compared to the wt receptor, whereas the $F113^{3.32}Y$ mutation resulted in only a 2-fold, non-significant decrease in potency (EC_{50} 0.219 ± 0.044 μM). In addition, the efficacy of ATP (**2**) was significantly different at the $F113^{3.32}A$ (185 ± 16%, $p \leq .0001$, ****) and the $F113^{3.32}Y$ (31 ± 7%, $p \leq .0001$, ****) mutants compared to that at the wt $P2Y_2R$ (set at 100%). Residues $Arg110^{3.29}$, $Phe113^{3.32}$ and to a lesser extent $Asp185^{ECL2}$ were observed to be important for $P2Y_2R$ activation by UTP and ATP.

3.3.1.3. Ap_4A. The EC_{50} value of Ap_4A (**3**) at the wt $P2Y_2R$ amounted to 0.0695 ± 0.0065 μM with 88% efficacy compared to UTP, similar to the previously reported values [50]. Ap_4A was completely inactive at most of the $P2Y_2R$ mutants (i.e. $R110^{3.29}A$, $F113^{3.32}A$, $F113^{3.32}Y$ and $D185^{ECL2}A$) except for the $F195^{5.35}Y$ mutant, at which it showed a 3-fold decrease in potency (EC_{50} 0.194 ± 0.043 μM, $p \leq .001$, ***), and a moderate reduction in efficacy to 67 ± 8% ($p \leq .05$, *) (see Figs. 7 and 8).

3.3.1.4. MRS4062. The wt $P2Y_2R$ was activated by the $P2Y_4R$ agonist MRS4062 (**5**) with an EC_{50} value of 0.535 ± 0.044 μM and 88 ± 4% efficacy compared to UTP. MRS4062 was 10-fold more potent at the $F113^{3.32}Y$ receptor mutant (EC_{50} 0.0546 ± 0.0145 μM, $p \leq .0001$, ****), 3-fold more potent at the $F195^{5.35}Y$ receptor mutant (EC_{50} 0.178 ± 0.027 μM, $p \leq .001$, ***) and completely inactive at all other investigated $P2Y_2R$ mutants (Figs. 7 and 8). MRS4062 showed reduced efficacies at the $F113^{3.32}Y$ mutant (20 ± 2%, $p \leq .0001$, ****) and at the $F195^{5.35}Y$ mutant (71 ± 3%, $p \leq .001$, ***) compared to the wt $P2Y_2R$.

3.3.2. Evaluation of agonists at the $P2Y_4R$

3.3.2.1. UTP. UTP displayed an EC_{50} value of 0.135 ± 0.025 μM at the wt *h*$P2Y_4R$. At the $P2Y_4R$ mutants, UTP showed no significantly different potency, except for the $R190^{ECL2}A$ mutant where it displayed a 15-fold decrease (EC_{50} 1.98 ± 0.20 μM, $p \leq .0001$, ****, see Figs. 9 and 10 and Table S3). However, differences in agonist efficacies were observed for several mutants (Fig. 11). Notably, there was a slight decrease in UTP potency at the $Y197^{5.35}A$ (0.411 ± 0.056 μM, 3-fold) and the $F200^{5.38}A$ (0.284 ± 0.018 μM, 2-fold) mutants with significantly reduced efficacy to 56 ± 6% ($p \leq .001$, ***) and 24 ± 5% ($p \leq .0001$, ****), respectively. UTP was least potent at the $R190^{ECL2}A$ mutant with a 15-fold decrease (EC_{50} 1.98 ± 0.20 μM, $p \leq .0001$, ****) and only 53 ± 6% efficacy ($p \leq .001$, ***) compared to the wt $P2Y_4R$ (100%).

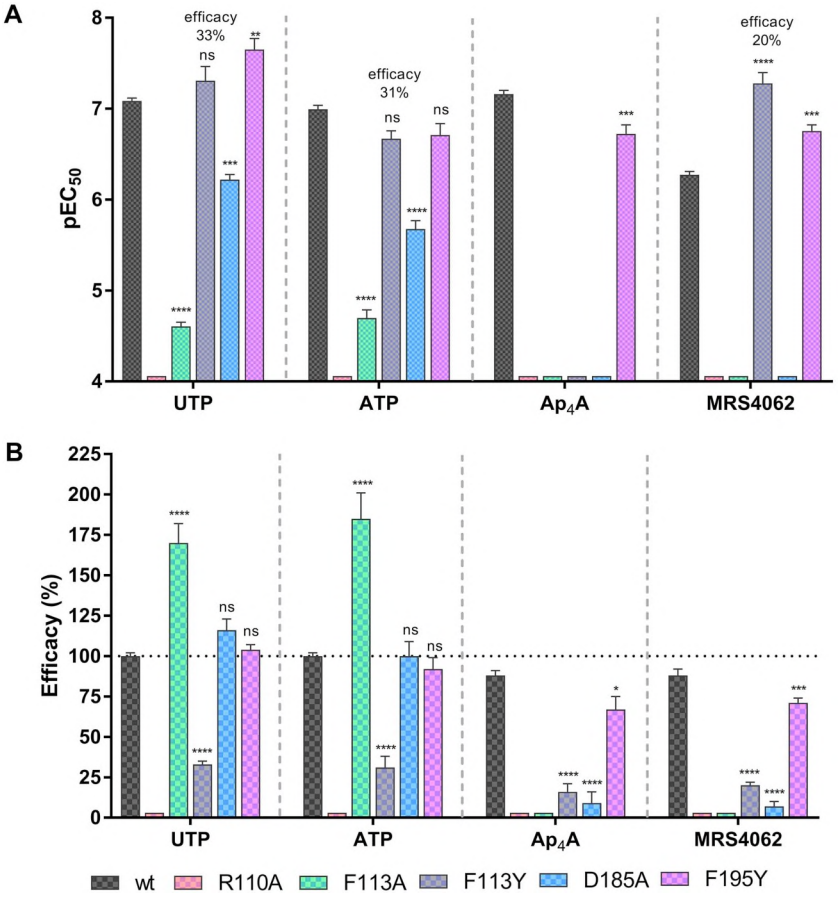

Fig. 8. A. Potencies and **B**. efficacies of the selected P2Y agonists determined in calcium mobilization assays on human wt and mutant $P2Y_2Rs$ expressed in 1321 N1 astrocytoma cells. Data represent means ± SEM (n = 4–6) performed in duplicates. One-way ANOVA with Dunnett's post-hoc test: ^{ns} not significant; * $p \leq .05$; ** $p \leq .01$; *** $p \leq .001$; **** $p \leq .0001$.

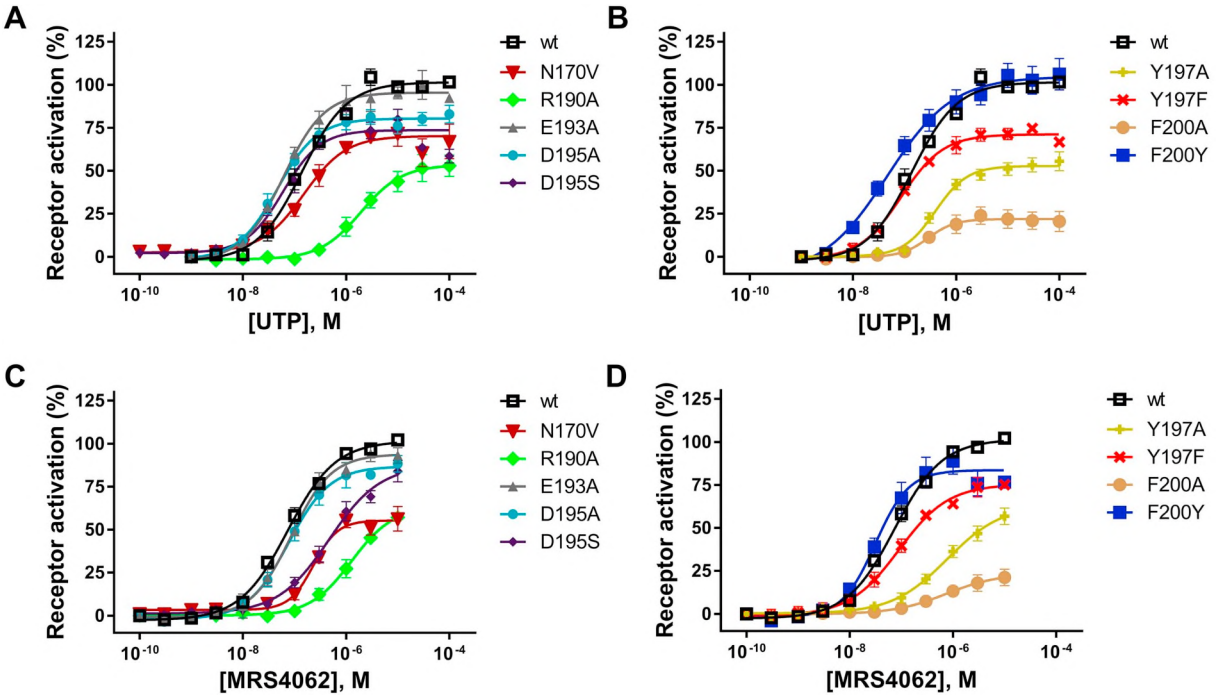

Fig. 9. Concentration–response curves of UTP (**A** and **B**) and MRS4062 (**C** and **D**) determined by calcium mobilization assays on the $P2Y_4Rs$ (wt and mutants) expressed in 1321 N1 astrocytoma cells. Each data point represents means ± SEM of 4–6 independent determinations each in duplicates. EC_{50} values are reported in Supplementary Table S3, pEC_{50} values are shown in Fig. 11.

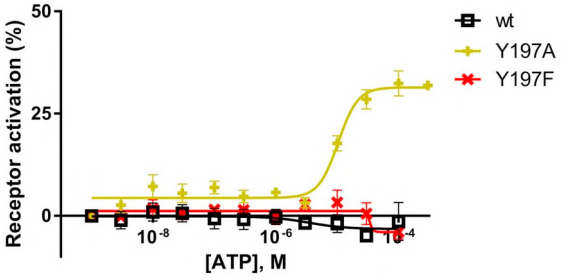

Fig. 10. Concentration–response curves of ATP on the wt $P2Y_4R$ and the $P2Y_4R$ mutants $Y197^{5.35}A$ and $Y197^{5.35}F$ expressed in 1321 N1 astrocytoma cells as determined in calcium mobilization assays. Replacement of $Tyr197^{5.35}$ in the wt $P2Y_4R$ by alanine ($Y197^{5.35}A$), but not by phenylalanine ($Y197^{5.35}F$), led to a receptor mutant that could be activated by ATP (EC_{50} 11.9 ± 1.6 μM) with an efficacy of 32 ± 3% compared to the maximal effect of UTP (100%). Each data point represents means ± SEM of 4–6 independent determinations each in duplicates. EC_{50} values are reported in Supplementary Table S3, pEC_{50} values are shown in Fig. 11.

3.3.2.2. ATP. ATP was inactive at the wt $P2Y_4R$ as previously described [2,12]. Interestingly, ATP showed some activity at the $P2Y_4R$ mutant $Y197^{5.35}A$ with an EC_{50} value of 11.9 ± 1.6 μM and an efficacy of 32 ± 3%, while it was inactive at all other investigated $P2Y_4R$ mutants (see Figs. 9 and 10, Table S3).

3.3.2.3. Ap_4A. In agreement with previous reports, Ap_4A (**3**) was completely inactive as an agonist at the wt *h*$P2Y_4R$, and the same was observed for its mutants (see Table S3 of Supplementary information) [2,12].

3.3.2.4. MRS4062. MRS4062 (**5**) was found in our experiments to be 7-fold selective for the wt $P2Y_4R$ (0.0761 ± 0.0100 μM, 100% efficacy) versus the wt $P2Y_2R$ (0.535 ± 0.044 μM, 88% efficacy) essentially confirming originally published data [44]. The potency of MRS4062 was significantly reduced at the $R190^{ECL2}A$ mutant (EC_{50} 1.24 ± 0.28 μM, 16-fold), the $Y197^{5.35}A$ mutant (EC_{50} 0.757 ± 0.068 μM, 10-fold), and the $F200^{5.38}A$ (EC_{50} 0.694 ± 0.069 μM, 9-fold) as compared to the wt $P2Y_4R$. The efficacies at these mutants were also significantly decreased to 57% ($p \leq .001$, ***) for the $R190^{ECL2}A$ and the $Y197^{5.35}A$ mutants, and to 21 ± 5% for the $F200^{5.38}A$ mutant ($p \leq .0001$, ****). MRS4062 showed also reduced efficacy at the $N170^{4.60}V$ receptor mutant (56 ± 7%, $p \leq .0001$, ****) although its potency was unchanged compared to the wt $P2Y_4R$ (see Figs. 9 and 11, Table S3).

3.4. Evaluation of antagonist potencies

Selected antagonists were tested in calcium assays at the wt $P2Y_2$- and $P2Y_4Rs$ and their mutants. Recombinant 1321 N1 cells were pre-incubated with different concentrations of antagonist followed by receptor stimulation by agonist at its EC_{80} concentration to obtain concentration-dependent inhibition curves. We tested the non-selective P2YR antagonist RB-2 (**6**), the related, but smaller AQ derivatives PSB-09144 (**9**), PSB-16133 (**10**), PSB-16135 (**11**) and PSB-1699 (**12**), as well as AR-C118925 (**7**) [34], a potent and selective $P2Y_2R$ antagonist derived from UTP. These antagonists have been proposed to bind to the orthosteric site of $P2Y_2R$ [50]. In contrast, at $P2Y_4R$, RB-2 and some other AQ derivatives were reported to bind to an allosteric pocket in close proximity to the orthosteric site, based on a computational study [47]. However, experimental evidence for this hypothesis is still lacking and the individual

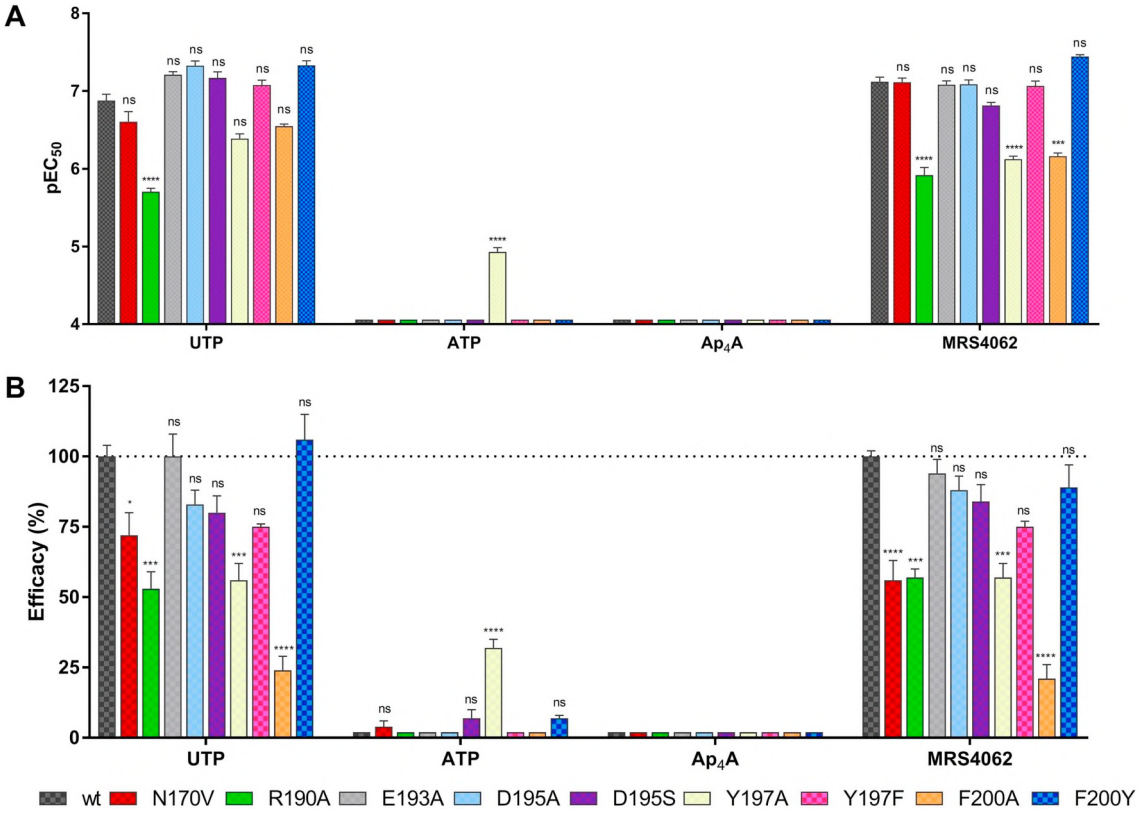

Fig. 11. A. Potencies and **B.** efficacies of selected P2Y agonists determined in calcium mobilization assays at the wt $P2Y_4R$ and its mutants expressed in 1321 N1 astrocytoma cells. EC_{50} values are presented in Supplementary Table S3. Data represent means ± SEM from 4 to 6 separate experiments performed in duplicates. Statistical analysis was done by one-way ANOVA with Dunnett's post-hoc test: ns not significant; * $p \leq .05$; ** $p \leq .01$; *** $p \leq .001$; **** $p \leq .0001$.

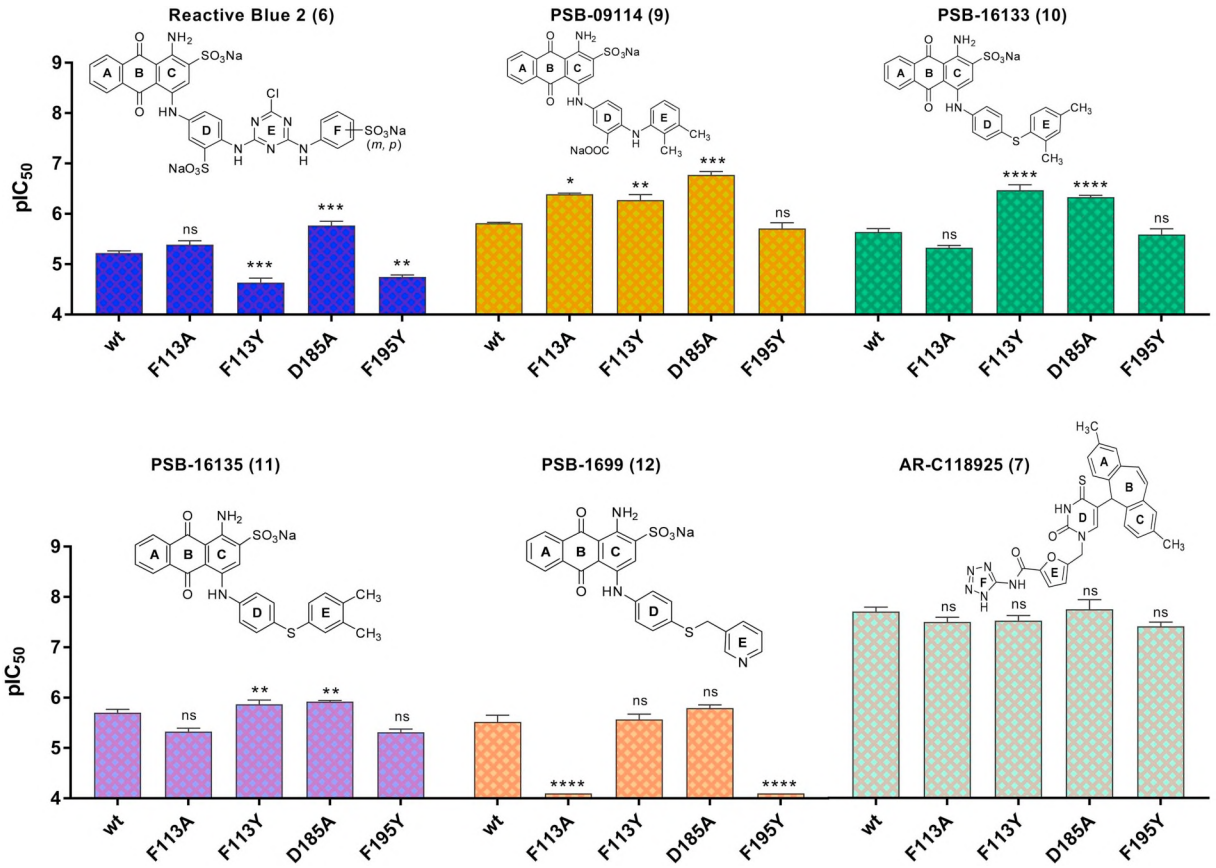

Fig. 12. Potencies of RB-2 (**6**, purified prior to testing), PSB-09114 (**9**), and PSB-16133 (**10**), PSB-16135 (**11**), PSB-1699 (**12**) and AR-C118925 (**7**) determined in calcium mobilization assays at the wt *h*P2Y$_2$R and its mutants expressed in 1321 N1 astrocytoma cells. Data represent mean pIC$_{50}$ values ± SEM of 3–5 independent determinations each in duplicates vs. UTP employed at its EC$_{80}$ value for the respective cell line. IC$_{50}$ values are reported in Supplementary Table S4. Concentration–response curves are shown in Supplementary Fig. S2.

interaction partners in the receptor protein have not been confirmed so far. Therefore, we set out to investigate the proposed differing binding modes of the AQ derivatives by our mutational approach (see Figs. 12 and 13 for potencies of the antagonists at the wt and mutant *h*P2Y$_2$- and *h*P2Y$_4$Rs; see Supplementary Information Fig. S2 and Table S4 for concentration–response curves and IC$_{50}$ values of antagonists at *h*P2Y$_2$R; for those at *h*P2Y$_4$R, see Supplementary Figs. S3 and S4, and Table S5).

3.4.1. Evaluation of antagonists at the P2Y$_2$R mutants

3.4.1.1. Reactive blue 2. At the wt P2Y$_2$R, the P2YR antagonist RB-2 displayed a potency in the low micromolar range (IC$_{50}$ 5.99 ± 0.563 μM) consistent with reported values [12,47]. We observed a 3- to 4-fold reduction in RB-2 potency at the mutants F113$^{3.32}$Y (IC$_{50}$ 23.5 ± 4.6 μM, $p \leq .0001$, ****) and F195$^{5.35}$Y (IC$_{50}$ 18.0 ± 1.5 μM, $p \leq .01$, **, Fig. 12). In contrast, RB-2 was 3-fold more potent at the D185^{ECL2}A mutant (IC$_{50}$ 1.73 ± 0.32 μM, $p \leq .001$, ***). RB-2 appeared to have a profile of inhibitory potency different from that of the other AQ derivatives at the P2Y$_2$R mutants studied (see Fig. 12).

3.4.1.2. Small anthraquinone derivatives. PSB-09114 (**9**), PSB-16133 (**10**) and PSB-16135 (**11**), showed no significant differences in potency at the wt P2Y$_2$R as compared to the mutant receptors F113$^{3.32}$A and F195$^{5.35}$Y. However, at the P2Y$_2$R mutants F113$^{3.32}$Y and D185^{ECL2}A, the potencies of these AQ derivatives, which are lacking ring F of RB-2, were significantly increased (see Fig. 12). PSB-09114 (**9**) was 3-fold more potent at the F113$^{3.32}$Y (IC$_{50}$ 0.550 ± 0.134 μM, $p \leq .05$, *) and 9-fold more potent at the D185^{ECL2}A receptor mutant (IC$_{50}$ 0.170 ± 0.025 μM, $p \leq .01$, **). Similarly, PSB-16133 (**10**) was 5- to 7-fold more potent, and PSB-16135 (**11**) was about 2-fold more potent at the F113$^{3.32}$Y (IC$_{50}$ 1.38 ± 0.26 μM, $p \leq .01$, **) and the D185^{ECL2}A (1.20 ± 0.06 μM, $p \leq .01$, **) mutants compared to the wt P2Y$_2$R (Fig. 12 and Table S4). Interestingly, the AQ derivative PSB-1699 (**12**), with a 2-atom linker between ring D and E, instead of a 1-atom linker as in **9–11**, showed a completely different pattern. Contrary to the AQ derivatives **9**–**11**, PSB-1699 (**12**, IC$_{50}$ 3.19 ± 0.97 μM at the wt P2Y$_2$R) showed no inhibition of UTP-induced receptor activation at the F113$^{3.32}$A and F195$^{5.35}$Y receptor mutants while it maintained potency similar to that at the wt P2Y$_2$R for the F113$^{3.32}$Y and D185^{ECL2}A receptor mutants.

3.4.1.3. AR-C118925. The potency of the UTP-derived P2Y$_2$R-selective antagonist AR-C118925 (**7**) was in the nanomolar range as previously reported [32]. Interestingly, there was no significant difference in AR-C118925 potency at the investigated P2Y$_2$R mutants (Fig. 12, also see Table S4 of Supplementary Information).

3.4.2. Evaluation of antagonists at the P2Y$_4$R mutants

3.4.2.1. Reactive-blue 2. RB-2 (**6**) was about 6-fold more potent at the wt P2Y$_4$R (IC$_{50}$ 1.05 ± 0.04 μM) as compared to the wt P2Y$_2$R (IC$_{50}$ 5.99 ± 0.563 μM). In comparison to the wt P2Y$_4$R, RB-2 was 2-fold less potent at the D195$^{5.33}$S mutant (2.26 ± 0.40 μM, $p \leq .05$, *), 3-fold less potent at the Y197$^{5.35}$F mutant (3.30 ± 0.65 μM, $p \leq .001$, ***) and 4-fold less potent at the F200$^{5.38}$Y mutant (4.17 ± 0.22 μM, $p \leq .0001$, ****). At the N170$^{4.60}$V mutant, RB-2 was 2-fold more potent (0.477 ± 0.083 μM, $p \leq .05$, *). There was no significant change in potency of RB-2 at the other investigated P2Y$_4$R mutants (see Fig. 13 and Table S5).

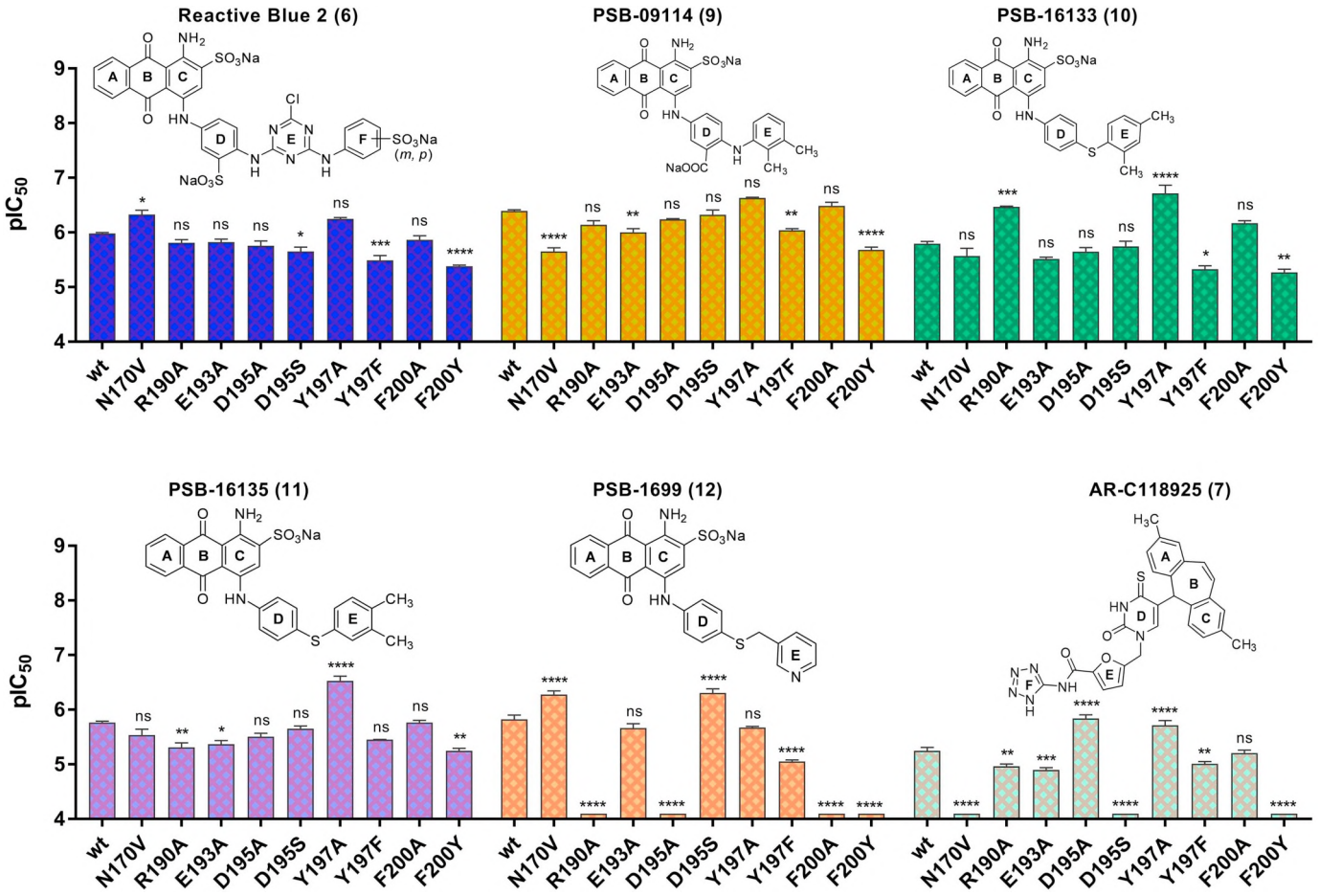

Fig. 13. Potencies of RB-2 (**6**, purified), PSB-09114 (**9**), and PSB-16133 (**10**), PSB-16135 (**11**), PSB-1699 (**12**) and AR-C118925 (**7**) as determined by calcium mobilization assays at the wt *h*P2Y$_4$R and its mutants expressed in 1321 N1 astrocytoma cells. Data represent mean pIC$_{50}$ values ± SEM of 3–5 independent determinations each in duplicates vs. UTP (at its EC$_{80}$ value for the respective cell line). IC$_{50}$ values are reported in Supplementary Table S5. Concentration–response curves are shown in Supplementary Fig. S3 and S4.

3.4.2.2. Small anthraquinone derivatives. No significant or only moderate differences between the potencies of PSB-09114 (**9**, IC$_{50}$ 0.403 ± 0.017 μM, wt *h*P2Y$_4$R), PSB-16133 (**10**, IC$_{50}$ 1.62 ± 0.17 μM, wt *h*P2Y$_4$R) and PSB-16135 (**11**, IC$_{50}$ 1.73 ± 0.11 μM, wt *h*P2Y$_4$R) at the wt P2Y$_4$R and the investigated P2Y$_4$R mutants were observed (see Fig. 13 and Table S5). PSB-09114 (**9**) was 5-fold less potent at the N170$^{4.60}$V (2.26 ± 0.35 μM, $p \leq .0001$, ****) and the F200$^{5.38}$Y (2.09 ± 0.24 μM, $p \leq .0001$, ****) mutants, and 2-fold less potent at the E193^{ECL2}A (1.01 ± 0.16 μM, $p \leq .01$, **) and the Y197$^{5.35}$F (0.913 ± 0.059 μM, $p \leq .01$, **) mutants compared to the wt P2Y$_4$R. PSB-16133 (**10**) showed a significant, 3-fold decrease in potency at the Y197$^{5.35}$F (4.77 ± 0.68 μM, $p \leq .05$, *) and the F200$^{5.38}$Y (5.43 ± 0.71 μM, $p \leq .01$, **) receptor mutants, whereas its potency increased by 5-fold at R190^{ECL2}A (0.339 ± 0.010 μM, $p \leq .001$, ***) and 8-fold at the Y197$^{5.35}$A mutant (0.205 ± 0.068 μM, $p \leq .0001$, ****). The potency of PSB-16135 (**11**) was 3-fold lower at the R190^{ECL2}A (4.98 ± 0.94 μM, $p \leq .01$, **), the E193^{ECL2}A (4.33 ± 0.65 μM, $p \leq .05$, *) and the F200$^{5.38}$Y (5.69 ± 0.62 μM, $p \leq .01$, **) receptor mutants. At the Y197$^{5.35}$A mutant, PSB-16135 displayed a 6-fold increase in potency (0.303 ± 0.060 μM, $p \leq .0001$, ****).

Interestingly, as observed at P2Y$_2$R, PSB-1699 (**12**) also displayed a different pattern as compared to the other AQ derivatives at the P2Y$_4$R subtype. PSB-1699's inhibitory potency (**12**, IC$_{50}$ 1.53 ± 0.27 μM, wt *h*P2Y$_4$R) was completely abolished at the R190^{ECL2}A, D195$^{5.33}$A, F200$^{5.38}$A, and F200$^{5.38}$Y receptor mutants. At the Y197$^{5.35}$F receptor mutant, there was a 6-fold decrease in potency while it was 3-fold more potent at the N170$^{4.60}$V (0.537 ± 0.084 μM, $p \leq .0001$, ****) and the D195$^{5.33}$S P2Y$_4$R mutants (0.504 ± 0.090 μM, $p \leq .0001$, ****) relative to the wt P2Y$_4$R.

3.4.2.3. AR-C118925. In the current study, AR-C118925 (**7**) was determined to be about 270-fold selective for P2Y$_2$R (IC$_{50}$ 0.0212 ± 0.0042 μM) over P2Y$_4$R (IC$_{50}$ 5.73 ± 0.82 μM). These data confirm the previously published selectivity profile of AR-C118925 (**7**) [32]. With the exception of F200$^{5.38}$A which showed no significant difference in potency of AR-C118925 relative to the wt P2Y$_4$R, the introduced mutations significantly affected AR-C118925 potency at P2Y$_4$R (Fig. 13). Most mutations led to a reduction in potency of the antagonist. The inhibitory potency of **7** versus UTP was completely lost in the N170$^{4.60}$V, D195$^{5.33}$S and F200$^{5.38}$Y receptor mutants. AR-C118925 showed a 2-fold decrease in potency at the R190^{ECL2}A (10.9 ± 1.01 μM, $p \leq .01$, **) and the E193^{ECL2}A mutants (12.7 ± 1.2 μM, $p \leq .001$, ***), two amino acids predicted to form ionic locks in P2Y$_4$R. In contrast, **7** was about 3- to 4-fold more potent at the D195$^{5.33}$A and the Y197$^{5.35}$A mutants than at the wt P2Y$_4$R with IC$_{50}$ values of 1.47 ± 0.22 μM ($p \leq .0001$, ****) and 1.96 ± 0.38 μM ($p \leq .0001$, ****), respectively.

3.5. Docking studies and assessment of mutagenesis data

3.5.1. Agonists at the hP2Y$_2$R

3.5.1.1. UTP. Docking studies of the selected agonists and antagonists were performed based on the X-ray crystal structure of the related P2Y$_1$R also taking into account the published structures of the somewhat more distantly related P2Y$_{12}$R subtype [49,52]. Results of

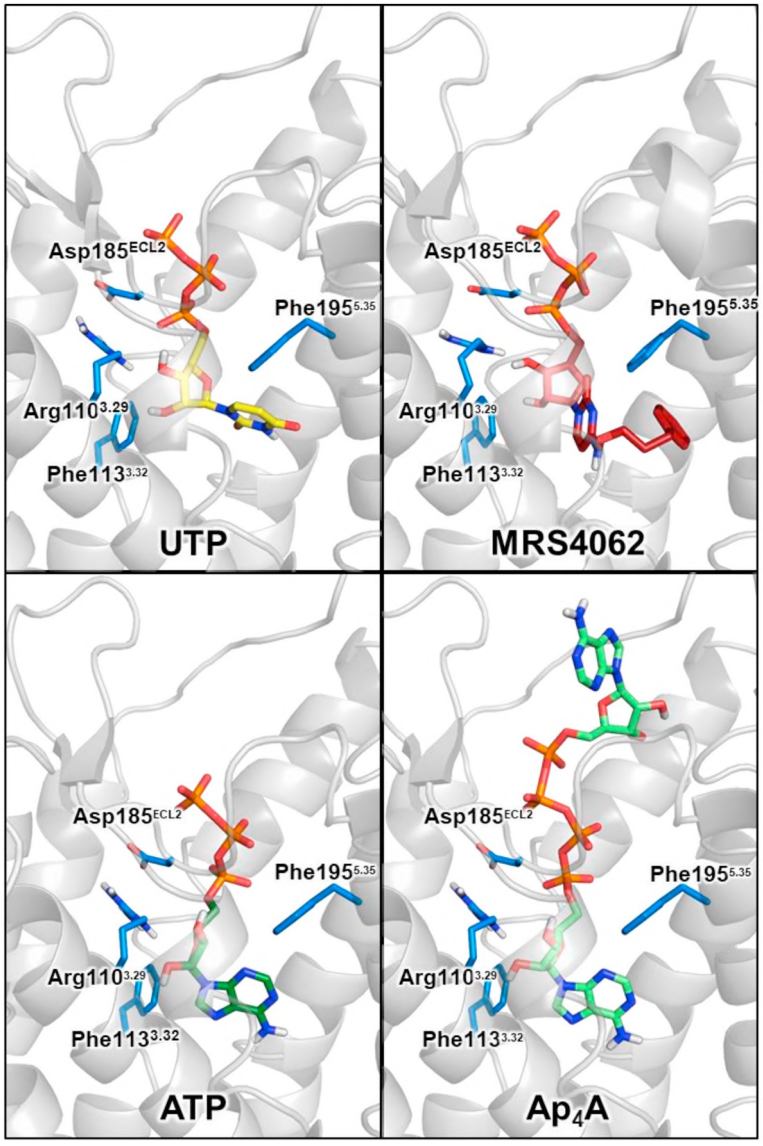

Fig. 14. Interactions of selected $P2Y_2R$ agonists docked into the putative binding pocket of $h P2Y_2R$ with amino acid residues that were exchanged in the present mutagenesis study. Carbon atoms of UTP are colored in yellow, of MRS4062 in dark red, of ATP in dark green, and of Ap_4A in light green. For further color code see Fig. 4.

the present as well as previously published mutagenesis studies provided additional important information to predict ligand–receptor interactions and receptor activation on a molecular level.

Interactions of the phosphate groups with charged amino acids ($Arg177^{ECL2}$, $His184^{ECL2}$, $Asp185^{ECL2}$, $Arg265^{6.55}$, $Arg272^{ECL3}$, $Lys289^{7.36}$, $Arg292^{7.39}$) and through hydrogen bonds ($Tyr268^{6.58}$, $Tyr269^{6.59}$) were predicted by the homology model of $h P2Y_2$ (see Fig. 4). The hydroxy groups of the ribose moiety likely form hydrogen bonds with $Arg110^{3.29}$ and $Asp185^{ECL2}$. The uracil base is accommodated in a binding pocket formed by several aromatic residues ($Phe113^{3.32}$, $Tyr114^{3.33}$, $Tyr118^{3.37}$, $Phe261^{6.51}$), where it is possibly stabilized through π–π-interactions and hydrogen bonding with the hydroxy groups of the tyrosine residues. UTP displayed an EC_{50} value of 82 nM at $h P2Y_2R$, which is consistent with previous reports in calcium assays [12,50]. In the present study, mutation of $Phe113^{3.32}$ to alanine resulted in a 300-fold decrease in potency of UTP (EC_{50} 25 ± 2.7 μM), while no significant differences were observed for the $F113^{3.32}Y$ mutant (EC_{50} 52.6 ± 18.3 nM), indicating that $Phe113^{3.32}$ might form π-π-interactions with the nucleobase. The mutation of $Asp204^{ECL2}$ in $h P2Y_1R$, a residue that is thought to be involved in an ionic lock with an arginine whose agonist-induced breaking contributes to the molecular receptor activation, had resulted in a 30-fold decrease in potency of the $P2Y_1R$ agonist 2-methylthio-ADP (2-MeSADP) [58]. A similar trend was observed for the analogous residue $Asp185^{ECL2}$ in $h P2Y_2R$, which resulted in a 7-fold decrease in UTP potency when mutated to alanine (EC_{50} 606 ± 76 nM). In accordance with our docking studies, the homologous exchange mutant $F195^{5.35}Y$ showed no negative effect on the potency of UTP (EC_{50} 23.3 ± 6.4 nM), which was predicted to interact with $Phe195^{5.35}$ through π–π-interactions.

3.5.1.2. ATP, Ap_4A. Docking studies suggested a binding mode for ATP similar to that of UTP and its derivative Ap_4A (see Fig. 14). The phosphate chain is supposed to bind in a pocket formed by positively charged residues, the same that were predicted to interact with the phosphate chain of UTP: $Arg177^{ECL2}$, $His184^{ECL2}$, $Asp185^{ECL2}$, $Arg265^{6.55}$, $Arg272^{ECL3}$, $Arg292^{7.39}$ (see Fig. 15). Interactions with those residues were previously confirmed [12,50,54]. ATP was about equipotent to UTP at the wt $h P2Y_2R$ (EC_{50} 102 nM) with nearly the same efficacy (see Table S2). The EC_{50} value of Ap_4A (**3**) at the wt $P2Y_2R$ amounted to 69.5 nM with 88% efficacy compared to UTP, similar to the previously reported values [50]. A complete loss of receptor activation had been observed for the $R265^{6.55}A$ and the $R292^{7.39}A$ $P2Y_2R$ mutants [50]. Mutation of

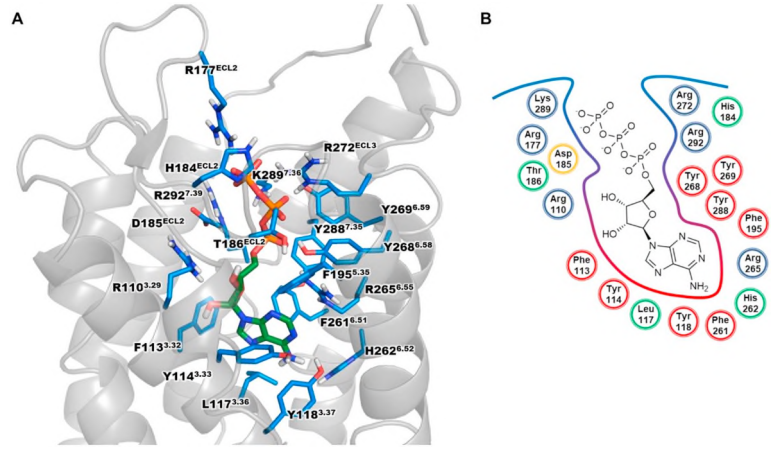

Fig. 15. Putative binding mode of ATP in the homology model of *h*P2Y$_2$R. **A**. Docked pose of ATP with the important residues in the binding pocket shown. Carbon atoms of ATP are colored in green. **B**. Schematic 2D representation of the binding pocket. For further color code see Fig. 4.

Arg272^{ECL3} to alanine was reported to lead to a 185-fold (ATP) and a > 4000-fold (Ap$_4$A) decrease in potency, respectively. The larger decrease in potency for Ap$_4$A versus ATP at the R272^{ECL3}A mutant [50] can be explained by additional interactions of the δ-phosphate group of Ap$_4$A. His184^{ECL2} may interact with one or several phosphate groups, as its mutation to alanine had resulted in a > 100-fold decrease in UTP and Ap$_4$A potency [50]. In the present study, differences between ATP and Ap$_4$A were observed at the D185^{ECL2}A mutant, which resulted in a 21-fold decrease in potency for ATP (EC$_{50}$ 2160 ± 454 nM), similar to the results for UTP, but it led to complete abolishment of receptor activation by Ap$_4$A (EC$_{50}$ > 10 μM). Ap$_4$A possesses an additional δ-phosphate located in close proximity to the putative ionic lock between Asp185^{ECL2} and Arg292$^{7.39}$ possibly allowing additional ionic and hydrogen bonding interactions that are not present in the ATP and UTP complex. Hydrogen bonds between phosphate groups of the nucleotides and tyrosine Tyr268$^{6.58}$, Tyr269$^{6.59}$ and Tyr288$^{7.35}$ are feasible (see Fig. 15). Previous findings support hydrogen bond interactions for Tyr268$^{6.58}$ and Tyr269$^{6.59}$, since mutation of those residues to phenylalanine had resulted in a > 10-fold decrease in UTP and Ap$_4$A potency [50]. Tyr288$^{7.35}$, on the other hand, might play a role in agonist discrimination. The mutation of Tyr288$^{7.35}$ to alanine had resulted in a > 1000-fold decrease in potency of both UTP and Ap$_4$A, whereas its mutation to phenylalanine had severely affected the potency of Ap$_4$A (> 1000-fold decrease) but not so much that of UTP (20-fold decrease) [50]. It had been hypothesized that Tyr288$^{7.35}$ might form interactions with Arg265$^{6.55}$ resulting in a rotamer of Arg265$^{6.55}$ required for agonist binding, or Tyr288$^{7.35}$ itself might recognize and guide the nucleobase of the agonists towards the lipophilic binding pocket through π-π-interactions [50]. Arg110$^{3.29}$ likely forms hydrogen bonds with both hydroxy groups of the ribose moiety, while the backbone of Asp185^{ECL2} possibly forms hydrogen bonds with the 3′-hydroxy group of the ribose moiety. As previously reported for UTP and Ap$_4$A [50] and presently confirmed, mutation of the key residue Arg110$^{3.29}$ to alanine also led to complete abolishment of ATP activity (EC$_{50}$ > 10 μM). According to the model, the adenine moiety of ATP and one adenine moiety of Ap$_4$A bind in an aromatic binding cavity formed by the previously described aromatic and lipophilic amino acids Phe113$^{3.32}$, Tyr114$^{3.33}$, Leu117$^{3.37}$, Tyr118$^{3.38}$, Phe195$^{5.35}$, and Phe261$^{6.51}$. The nucleobases of ATP and Ap$_4$A are likely to form π-π-interactions with Phe113$^{3.32}$, since mutation of this residue to alanine resulted in a 200- and > 1000-fold decrease in potency for ATP (EC$_{50}$ 20.5 ± 4.2 μM) and Ap$_4$A (EC$_{50}$ > 10 μM), respectively. This is supported by the observation that the F113$^{3.32}$Y mutation had no significant effect on ATP potency (EC$_{50}$ 219 ± 44 nM). The decrease in potency for Ap$_4$A (EC$_{50}$ > 10 μM) might be due to different modes of receptor activation (as discussed below). Mutation of Phe195$^{5.35}$ to tyrosine also had no effect ATP potency and efficacy, whereas potency and efficacy of Ap$_4$A were slightly decreased (EC$_{50}$ 194 ± 43 nM). As we did not observe different interactions of Ap$_4$A and ATP within the ATP binding site of the model, the small difference in agonist potency might be explained by modulation of ECL2 flexibility resulting in weaker interactions with the larger agonist Ap$_4$A. The Y114$^{3.33}$F and F261$^{6.51}$A mutations had been reported to lead to complete abolishment of receptor activation by Ap$_4$A but not by UTP, which was explained by different interaction patterns of the nucleobases in the lipophilic binding domain [50]. The proposed ATP binding mode and interactions are presented in Fig. 15 which is consistent with all present and previously published experimental data.

The larger ATP derivative Ap$_4$A additionally projects into the extracellular domain of P2Y$_2$R (see Fig. 14). The δ-phosphate group might be involved in ionic interactions with Arg26$^{N\text{-terminus}}$ and Arg177^{ECL2} (not shown). Cation–π-interactions are conceivable between Arg24$^{N\text{-terminus}}$, Arg26$^{N\text{-terminus}}$, and Arg177^{ECL2} and the second adenine moiety forming a possible second nucleotide binding pocket close to the N-terminus and the extracellular domain. Mutation of Arg177^{ECL2} to alanine in previous studies had resulted in weaker effects on the potency of ATP (3-fold reduction in potency) as compared to Ap$_4$A (7-fold reduction) [12]. However, other binding modes of the second adenine group cannot be excluded.

3.5.1.3. MRS4062. The synthetic UTP-derivative MRS4062 (**5**), a moderately potent P2Y$_4$R agonist, is proposed to share the same binding site as the endogenous agonists (see Fig. 16). The wt P2Y$_2$R was activated by the P2Y$_4$R agonist MRS4062 (**5**) with an EC$_{50}$ value of 535 ± 44 nM and 88% efficacy compared to UTP. The interaction pattern of the phosphate groups is likely shifted due to the large N^4-substituent on the cytosine heterocycle. The α-phosphate may form ionic and hydrogen bonding interactions with Arg110$^{3.29}$, Lys289$^{7.36}$ and Arg292$^{7.39}$. The β-phosphate group possibly interacts with Asp185^{ECL2}, Tyr268$^{6.58}$, Lys289$^{7.36}$, and Arg292$^{7.39}$, and the γ-phosphate may form interactions with Arg177^{ECL2}, Asp185^{ECL2}, Arg272^{ECL3}, Lys289$^{7.36}$, and Arg292$^{7.39}$.

The potency of MRS4062 was decreased by > 100-fold at the D185^{ECL2}A mutant (EC$_{50}$ > 10 μM) compared to a 21-fold decrease for UTP, which may be explained by stronger interactions of MS4062 with Asp185^{ECL2} due to its shifted binding mode as compared to UTP. According to the docking study, the ribose moiety of MRS4062 might form hydrogen bonds between the 3′-hydroxy group and Arg110$^{3.29}$. As observed for UTP, ATP and Ap$_4$A, MRS4062 also could not activate the R110$^{3.29}$A mutant (EC$_{50}$ > 10 μM). The potency of MRS4062 was decreased by > 100-fold at the F113$^{3.32}$A mutant (EC$_{50}$ > 10 μM) and significantly increased (10-fold) at the F113$^{3.32}$Y mutant (EC$_{50}$ 54.6 ± 14.5 nM), likely due to the closer proximity of the nucleobase

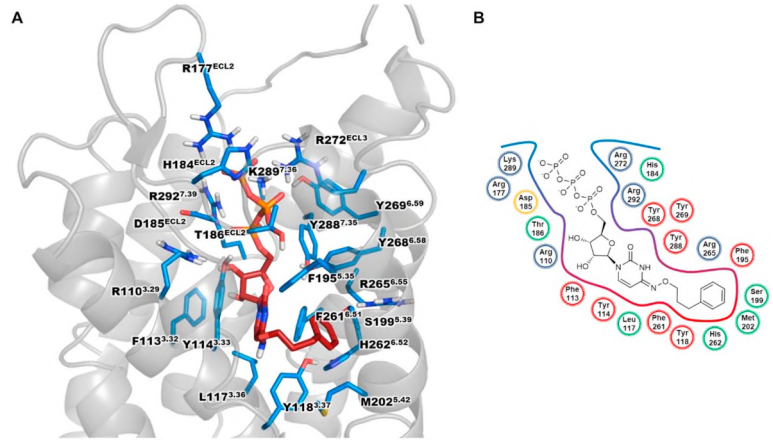

Fig. 16. Putative binding mode of MRS4062 in the homology model of *h*P2Y$_2$R. **A**. Docked pose of MRS4062 with the important residues in the binding pocket shown. Carbon atoms of MRS4062 are colored in red. **B**. Schematic 2D representation of the binding pocket. For further color code see Fig. 4.

to Phe113$^{3.32}$. The cytosine core is possibly stabilized through π–π-stacking with an induced rotamer of Tyr114$^{3.33}$, and the oxime substituent may project towards TM V. Several aromatic (Tyr118, Phe195$^{5.35}$, Tyr198) and lipophilic (Val168, Met202$^{5.42}$, Leu203) amino acid residues could be responsible for binding of the phenylpropyl residue through lipophilic interactions. The 3-fold increase in MRS4062 potency at the F195$^{5.35}$Y mutant (EC$_{50}$ 178 ± 27 nM) might be rationalized by additional hydrogen bonds between the introduced hydroxy group of the tyrosine and the keto group in position 2 of the cytosine moiety. In our docking studies, the phosphate chain still binds in the same cationic binding cavity as UTP, ATP and Ap$_4$A, whereas the nucleobase binding pocket of the cognate agonists is now occupied by the phenylpropyl residue of MRS4062, while the pyrimidine moiety is moved towards Phe113$^{3.32}$ and Tyr114$^{3.33}$.

3.5.1.4. Comparison of agonists. The efficacy profiles at the P2Y$_2$R mutants were similar between the agonists UTP and ATP on the one hand, and Ap$_4$A and MRS4062 on the other hand (see Fig. 8). The mutations F113$^{3.32}$A and D185^{ECL2}A resulted in very different effects as shown in Figs. 7 and 8. The F113$^{3.32}$A mutation caused a significant increase in efficacy in the case of UTP and ATP (170 ± 12 and 185 ± 16%, respectively), and a complete absence of receptor response for Ap$_4$A and MRS4062. Since ATP and Ap$_4$A likely share the same binding mode based on the collected data, the difference in their pharmacological profiles can be explained by different modes of receptor activation. This includes additional ionic and hydrogen bond interactions for Ap$_4$A involving the ionic lock between Asp185^{ECL2} and Arg292$^{7.39}$ and other residues close to the ionic lock. Further support for this hypothesis is provided by a decrease in efficacy of Ap$_4$A and MRS4062 at the D185^{ECL2}A mutant (9 ± 7 and 7 ± 3%, respectively), while no changes in efficacies for UTP and ATP could be observed for that mutant (116 ± 7 and 100 ± 9%, respectively). It is possible, that the formation of the ionic lock between Asp185^{ECL2} and Arg292$^{7.39}$ induces a specific rotamer of Arg292$^{7.39}$ which is needed for interaction with the phosphate groups. Since Ap$_4$A possesses an additional δ-phosphate group, and MRS4062 likely has a slightly different interaction pattern due to its shifted position in the binding pocket, they might form additional interactions with the rotamer of Arg292$^{7.39}$, which are not present in the case of UTP and ATP.

Although no significant changes in potencies and efficacies of agonists were determined for the F195$^{5.35}$Y mutant, different trends were observed depending on the agonist structure. When mutated to tyrosine, the potency of UTP and MRS4062 slightly increased while it decreased for ATP and Ap$_4$A with respect to the wt P2Y$_2$R. Our docking studies suggest that the nucleobase binds close to Phe195$^{5.35}$ which would allow π-π-interactions of varying magnitudes with the adenine and uracil derivatives, respectively. Since the space in the investigated lipophilic binding pocket is limited, the size and functionality of residues might be crucial for ligand discrimination. The Phe195$^{5.35}$ residue is conserved in the mouse and rat P2Y$_2$R, but exchanged for the larger tyrosine residue in the mouse, rat and *h*P2Y$_4$R (Tyr197$^{5.35}$). Mutation of Tyr197$^{5.35}$ to alanine introduced ATP-sensitivity into P2Y$_4$R, probably due to the increase in available space, but since it was not crucial for ATP agonism at P2Y$_2$R, we expect several residues besides Phe195$^{5.35}$ to be responsible for accepting both ATP and UTP by P2Y$_2$R.

3.5.2. Antagonists at the hP2Y$_2$R

3.5.2.1. Anthraquinone derivatives. The AQ derivatives are proposed to bind in the upper third part of P2Y$_2$R (see Fig. 17). While rings A and B of AQs (Fig. 2) are exposed towards the extracellular space, the sulfonate group of ring C likely forms ionic and hydrogen bond interactions with charged residues, such as Arg110$^{3.29}$, Lys289$^{7.36}$ and Arg292$^{7.39}$. Increased potencies (2- to 9-fold) of the investigated AQ-derived antagonists were determined at the D185^{ECL2}A mutant. The mutation of Asp185^{ECL2} to alanine would break the ionic lock with Arg292$^{7.39}$ thus allowing rotamers to form additional interactions with the sulfonate of AQ ring C. Ring D probably binds in a cavity formed by the aromatic residues Tyr268$^{6.58}$, Tyr269$^{6.59}$ and Tyr288$^{7.35}$. Mutation of Tyr269$^{6.59}$ to phenylalanine had resulted in increased potency for small AQ derivatives with lipophilic substitutions on ring E [50]. Ring E likely projects into the putative orthosteric binding site, overlapping with the nucleobase binding cavity of the agonists. Several lipophilic (Leu117$^{3.36}$) and aromatic residues (Phe113$^{3.32}$, Tyr114$^{3.33}$, Phe261$^{6.51}$, Tyr269$^{6.59}$) may be involved in stabilizing ring E in the orthosteric binding site. Additional cation-π-interactions are feasible with Arg265$^{6.55}$. Mutation of Phe113$^{3.32}$ to alanine had no significant effect on the potency of the antagonists except for PSB-1699 (**12**), which showed a complete loss of antagonistic activity at the F113$^{3.32}$A mutant (IC$_{50}$ > 10 μM). In the case of PSB-1699, the distance between Phe113$^{3.32}$ and ring E amounts to approximately 3.6 Å according to our model, which is a reasonable distance for π-π-interactions. In the complexes of the other AQ antagonists, PSB-16133 (**10**) and PSB-16135 (**11**), the distance between ring E and Phe113$^{3.32}$ was estimated to be 5.1 Å, leading to the assumption that no π–π-interactions can be formed. π–π-Interactions between ring E of PSB-1699 and Phe113$^{3.32}$ are further supported by the fact that the F113$^{3.32}$Y mutant showed no decrease in potency (IC$_{50}$ 2770 ± 654 nM). In our previously published study [50], the Y114$^{3.33}$F mutation located deep down in the orthosteric binding pocket, had resulted in increased potency of several AQ derivatives, but had no effect on the larger RB-2. The Y114$^{3.33}$A mutant, on the other hand, had led to significantly decreased potency of RB-2, but had not shown any effect on the potency of small AQ derivatives [50]. This further supports the

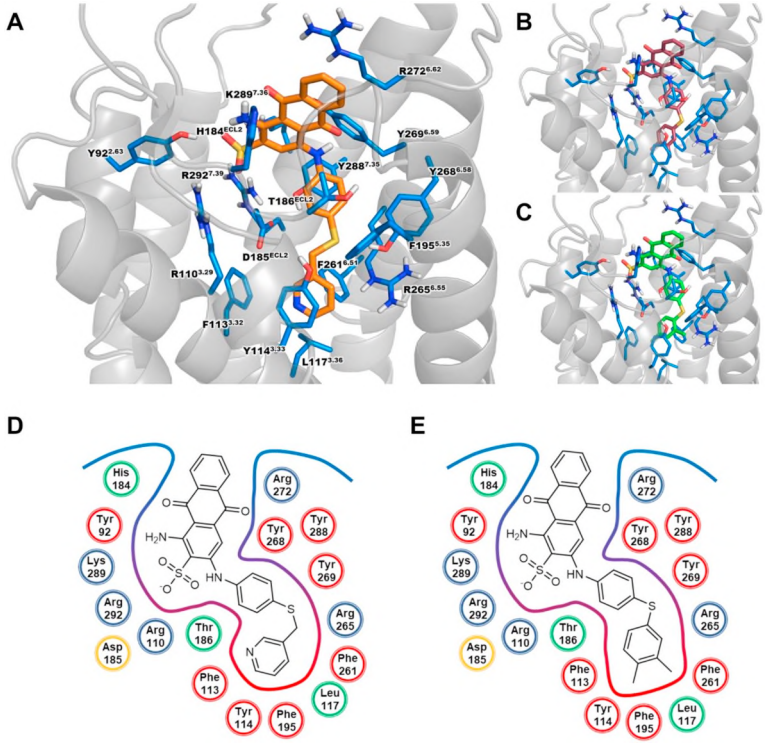

Fig. 17. Putative binding mode of selected AQ-derived antagonists in the homology model of *h*P2Y$_2$R. **A**. Docked pose of PSB-1699 with the important residues in the binding pocket shown. The h2Y$_2$R (gray) is displayed in cartoon representation, the amino acid residues (blue) and PSB-1699 (orange) are shown as stick models. Oxygen atoms are colored in red, nitrogen atoms in blue, phosphorus atoms in orange, sulfur atoms in yellow. **B**. Binding mode of PSB-16133. **C**. Binding mode of PSB-16135. Schematic 2D representation of the binding pocket of PSB-1699 (**D**) and PSB-16133 (**E**). Charged, basic residues are circled in blue, aromatic residues in red, the conserved aspartic acid residue in ECL2 involved in the ionic lock in yellow, and further residues in the binding pocket in green (in **D**, **E**).

proposed binding mode of small AQ derivatives in the orthosteric binding pocket, but not that of the larger RB-2 having an additional ring F with a charged sulfonate group. A complete loss of inhibitory potency of PSB-1699 was also observed at the F195$^{5.35}$Y mutant close to the orthosteric binding site (IC$_{50}$ > 10 μM), while the potency of RB-2 was decreased (3-fold, IC$_{50}$ 18.0 ± 1.54 μM), and the potency of the other investigated AQ derivatives PSB-09114 (**9**), PSB-16133 (**10**), and PSB-16135 (**11**) remained unaffected (IC$_{50}$ 2020 ± 513, 2660 ± 683, 4890 ± 708 nM, respectively). The longer linker in PSB-1699 between ring D and E increases the flexibility of the molecule and may thereby allow π–π-interactions with Phe195$^{5.35}$. The replacement of the phenylalanine with a tyrosine in the F195$^{5.35}$Y mutant introduces an additional hydroxy group which reduces the lipophilicity and limits the space in the binding cavity for ring E. As previously proposed by our group, the larger RB-2, with an additional sulfonated ring F, appears to have a different binding mode compared to the smaller AQ derivatives lacking that ring. No final docking predictions for the moderately potent RB-2 at *h*P2Y$_2$R are provided, as the interactions appear to be complex, and multiple binding modes cannot be excluded.

3.5.3. *Agonists at hP2Y$_4$R*

3.5.3.1. UTP. UTP displayed an EC$_{50}$ value of 135 ± 25 nM at the wt *h*P2Y$_4$R. UTP is predicted to bind in the upper third part of P2Y$_4$R, close to the ECL2, comparable to its binding mode at P2Y$_2$R (see Fig. 4). According to the model, phosphate groups are accommodated in a negatively charged binding cleft formed by Lys34$^{1.31}$, Lys289$^{7.36}$, and Arg292$^{7.39}$. Residues likely involved in forming hydrogen bonds with the phosphate groups include Asp187^{ECL2}, Tyr268$^{6.58}$, and Asn285$^{7.32}$. The 2′- and 3′-hydroxy groups probably form hydrogen bonding interactions with Arg112$^{3.29}$, and the 5′-hydroxy group might form additional hydrogen bonds with the backbone of Asp185. The oxygen atom of the ribose ring may form a hydrogen bond with Tyr288$^{7.35}$. The uracil moiety is predicted to bind in a lipophilic region consisting of aromatic (Phe115$^{3.32}$, Tyr116$^{3.33}$, Tyr120$^{3.37}$, Tyr197$^{5.35}$, Phe200$^{5.38}$, Phe261$^{6.51}$) and lipophilic (Leu119$^{3.37}$, Val204$^{5.42}$, Met205$^{5.43}$) residues. Cation-π-interactions between the uracil moiety and Arg265$^{6.55}$ are conceivable. Small decreases (2–3-fold, not quite reaching the level of statistical significance) in UTP potency were observed for the Y197$^{5.35}$A (EC$_{50}$ 411 ± 56 nM) and F200$^{5.38}$A (EC$_{50}$ 284 ± 18 nM) mutants. The Y197$^{5.35}$F and F200$^{5.38}$Y mutants with preserved aromatic functionality had no effect on UTP potency, supporting π–π-interactions with the nucleobase (Fig. 4). Arg194$^{5.34}$ of P2Y$_2$R had been reported to be important for agonist potency [50], indicating indirect modulation rather than direct interaction between the agonist and the amino acid side-chain, e.g. by the increased flexibility of the ECL2 resulting in different receptor conformations; it had been proposed to be involved in a second ionic lock distant from Asp185^{ECL2} and Arg292$^{7.39}$.

A significant change in UTP potency was observed for the mutant of the corresponding amino acid in P2Y$_4$R, R190^{ECL2}A (15-fold decrease in potency, EC$_{50}$ 1980 ± 196 nM), while no changes were observed for the E193^{ECL2}A (EC$_{50}$ 61.6 ± 5.2 nM) and the D195$^{5.33}$A/S mutants (EC$_{50}$ 47.5 ± 6.6 nM and 68.6 ± 12.0 nM, respectively). Although distant from the orthosteric binding site, we could neither confirm Glu193^{ECL2} nor Asp195$^{5.33}$ as major interaction partners for Arg190^{ECL2} to form an ionic lock. Other residues in TM V such as Glu192^{ECL2} might act as ionic interaction partners for Arg190^{ECL2}. Mutation of Asn170$^{4.60}$ of P2Y$_4$R, which is a non-conserved amino acid residue in the P2Y$_2$- and P2Y$_4$Rs, had no effect on UTP potency.

Our docking results support a similar binding mode of UTP at P2Y$_2$- and P2Y$_4$Rs. In both cases several residues form a highly charged and hydrophilic binding cleft ideally suited for the binding of the phosphate chain, a slightly less hydrophilic binding pocket for the binding of the ribose where Arg$^{3.29}$ (P2Y$_2$-Arg110$^{3.29}$, P2Y$_4$-Arg112$^{3.29}$) probably forms bidentate hydrogen bonds with the 2′- and 3′-hydroxy groups, and a lipophilic pocket with an aromatic network as a binding site for the nucleobase.

3.5.3.2. ATP. The wt *h*P2Y$_4$R is activated by UTP but not by ATP (EC$_{50}$ > 10 μM). We were able to introduce ATP-sensitivity into P2Y$_4$R by mutating the large Tyr197$^{5.35}$ to alanine (EC$_{50}$ 11.9 ± 1.56 μM). The tyrosine residue in position 5.35 is conserved in the mouse, rat and human P2Y$_4$R. It is exchanged for a phenylalanine in P2Y$_2$R. However, mutation of Tyr197$^{5.35}$ in *h*P2Y$_4$R to phenylalanine did not result in ATP recognition. As discussed above, the aromatic side-chain in the 5.35 position might be involved in π–π-interactions with the nucleobase.

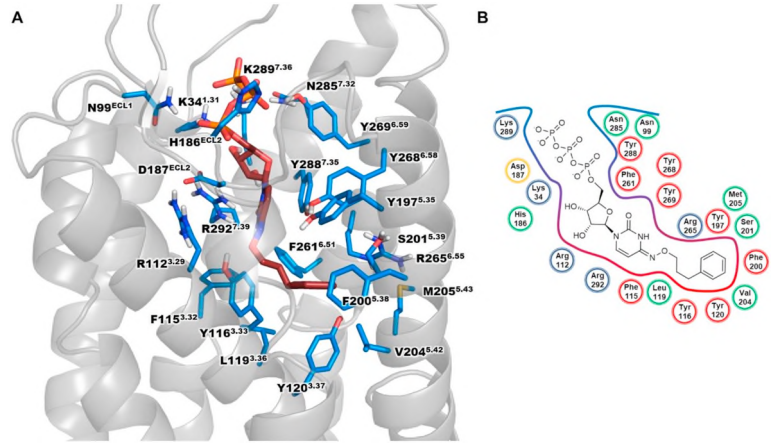

Fig. 18. Putative binding mode of the potent $P2Y_4R$ agonist MRS4062 in the homology model of *h*$P2Y_4R$. **A**. Docked pose of MRS4062 with the important residues in the binding pocket shown. Carbon atoms of MRS4062 are colored in red. **B**. Schematic 2D representation of the binding pocket. For further color code see Fig. 4.

Similar interactions are likely for Phe195$^{5.35}$ in $P2Y_2R$ with agonists. Our results indicate that Tyr197$^{5.35}$ may be too large and thereby prevent binding of the larger nucleobase adenine of ATP to the $P2Y_4R$. But Tyr197$^{5.35}$ is not solely responsible for the agonist preferences of the $P2Y_4R$. ATP-sensitivity of the $P2Y_4R$-Y197$^{5.35}$A mutant may also arise from altered flexibility of the ECL2 facilitating the binding of ATP.

The docking results based on the improved homology model indicate that the available space in the orthosteric binding domain is an important factor governing ligand recognition for both investigated receptors. At $P2Y_4R$, Met205$^{5.43}$ likely appears to be directed towards TM VI, while in $P2Y_2R$ the homologous Met202$^{5.42}$ is directed towards TM IV (see Supplementary Information, Fig. S5). Several rotamer combinations are possible for Met205$^{5.43}$ and Arg265$^{6.55}$ (numbered 265 in both receptors, see Fig. 4), in which they interact through hydrogen bonds resulting in an overall reduced space in the orthosteric binding site. At $P2Y_2R$, more rotamers of Arg265$^{6.55}$ are conceivable, as Met202$^{5.42}$ projects outwards of the orthosteric binding site, where it can form interactions with Cys164(4.56) and Gln165(4.57). In our previous studies we reported on the role of Arg265$^{6.55}$ and Tyr288$^{7.35}$ of *h*$P2Y_2R$ in UTP and Ap_4A binding [50]. The R265$^{6.55}$A and Y288$^{7.35}$A mutants were both insensitive towards UTP and Ap_4A. Interestingly, UTP was still accepted by the Y288$^{7.35}$F mutant, while Ap_4A failed to activate that mutant. We measured a volume of 310 Å^3 available in the binding site of $P2Y_2R$, and 220 Å^3 in the case of $P2Y_4R$, which leads to the assumption that the triad of Met202$^{5.42}$–Arg265$^{6.55}$–Tyr288$^{7.35}$ induces a rotamer of Arg265$^{6.55}$ in $P2Y_2R$ which provides the required space for binding of adenine nucleotides. The larger available space in the $P2Y_4R$–Y197$^{5.35}$A mutant could therefore be a reason for accepting the more spacious agonist ATP, which is completely inactive in the wt $P2Y_4R$.

3.5.3.3. MRS4062. MRS4062 (**5**) was found in our experiments to be 7-fold selective for the wt $P2Y_4R$ (EC_{50} 76.1 ± 10 nM, 100 ± 2% efficacy) versus the wt $P2Y_2R$ (EC_{50} 535 ± 44 nM, 88 ± 4% efficacy) essentially confirming originally published data [44]. According to the *h*$P2Y_4R$ model, MRS4062 (**5**) occupies the same binding pocket as UTP (see Fig. 18). The phosphate groups are proposed to form ionic or hydrogen bonding interactions with Glu31$^{N\text{-term}}$, Lys34$^{1.31}$, Asn99^{ECL1}, His186^{ECL2}, Asp187^{ECL2}, Tyr268$^{6.58}$, Arg272^{ECL3}, Asn285$^{7.32}$, Lys289$^{7.36}$, and Arg292$^{7.39}$. In the model, the ribose moiety binds close to TM I and VII, where the 5′-hydroxy group might form hydrogen bonding interactions with Lys34$^{1.31}$. The uracil moiety likely forms hydrogen bond interactions with Arg292$^{7.39}$, while other aromatic residues (Phe115$^{3.32}$, Phe261$^{6.51}$, Tyr288$^{7.35}$) may stabilize the nucleobase through π-π-interactions. The phenylpropyl residue is predicted to occupy the nucleobase binding cavity at the bottom of the orthosteric binding site. According to the model, the phenyl group binds close to several aromatic residues, including Tyr116$^{3.33}$, Tyr120$^{3.37}$, Tyr197$^{5.35}$ and Phe200$^{5.38}$, whereas other residues (Leu119$^{3.37}$, Val204$^{5.42}$, Phe261$^{6.51}$) increase the lipophilicity in the binding cavity. The phenylpropyl group of MRS4062 is accommodated in the putative nucleobase binding domain, and the pyrimidine moiety is shifted in $P2Y_4R$ as in $P2Y_2R$, leading to similar binding modes in both receptor subtypes. In the $P2Y_4R$ docking studies, MRS4062 displayed a somewhat larger shift towards TM VII than in $P2Y_2R$. The R190^{ECL2}A mutant showed a significant decrease (16-fold, EC_{50} 1240 ± 279 nM) in agonist potency compared to the wt $P2Y_4R$, most likely due to the altered flexibility of the ECL2. Larger decreases in potency were also observed for the Y197$^{5.35}$A (10-fold, EC_{50} 757 ± 68 nM) and F200$^{5.38}$A mutants (9-fold, EC_{50} 694 ± 69 nM), indicating that the phenylpropyl substitution might contribute to stronger π–π-interactions with the two residues as compared to UTP. This is supported by the Y197$^{5.35}$F and F200$^{5.38}$Y mutations, which had no effect on the potency of MRS4062.

Previously, Marouka, Jacobson *et al.,* who had developed MRS4062, reported on its selectivity for *h*$P2Y_4$ over $P2Y_2R$. Based on a homology model of the two receptors generated based on the X-ray crystal structure of the CXCR4 chemokine receptor, they predicted that the phenyl moiety of the N^4-phenylpropoxy group of MRS4062 projects from the $P2Y_4R$ binding pocket into a cavity formed by the ECL2 surrounded by Thr182^{ECL2} and Leu184^{ECL2}. According to that study, the cavity is surrounded by bulky amino acids, Arg180^{ECL2} and Thr182^{ECL2}, in $P2Y_2R$ which was put forward as a possible explanation for the $P2Y_4R$-selectivity of MRS4062 [44]. Our current results, based on the recently published X-ray structure of the more closely related $P2Y_1R$, indicate that MRS4062, like UTP, has a binding mode similar to that observed for nucleotide agonists in the X-ray structure of *h*$P2Y_{12}R$ [52]. The previous and current mutagenesis data, however, cannot completely explain the $P2Y_4R$-selectivity of MRS4062.

3.5.4. Antagonists at *hP2Y*$_4$*R*

3.5.4.1. Anthraquinone derivatives. As previously reported, the AQ derivatives had been predicted to bind in the upper third part of *h*$P2Y_4R$ [47]. The small AQ derivatives were proposed to bind close to the ECL2 where the 2-sulfonate of ring C can interact with charged residues (Lys34$^{1.31}$, Asp187^{ECL2}, Arg292$^{7.39}$) comparable to the binding position of the same 2-sulfonate group in $P2Y_2R$ (see Fig. 19). Ring D of AQs is presumably stabilized by interactions with His186^{ECL2} and Tyr288$^{7.35}$. Ring E may bind close to TM V and VI in a highly aromatic binding pocket formed by Tyr116$^{3.33}$, Tyr197$^{5.35}$, Phe200$^{5.38}$, Tyr269$^{6.59}$, where it is stabilized through π-π-stacking with, and probably through cation–π-interactions with Arg265$^{6.55}$. In the case of RB-2, a similar binding mode was proposed. The 3-sulfonate of ring D likely interacts with charged residues (Lys34$^{1.31}$, Asp187^{ECL2}, Arg292$^{7.39}$) and ring F was

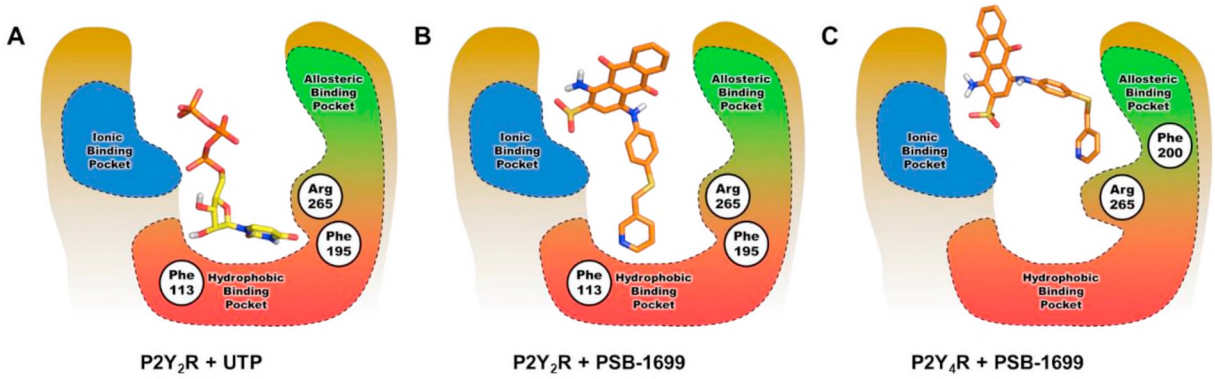

Fig. 19. Comparison of agonist (**A**) and antagonist binding modes in the $P2Y_2$- (**B**) and $P2Y_4R$ pocket (**C**). Carbon atoms of UTP are colored in yellow, those of PSB-1699 in orange. Negatively charged groups of the ligands interact with a binding cavity consisting of positively charged amino acid residues denoted as 'ionic binding pocket'. The putative orthosteric binding pocket is located beneath ECL2 and consists of lipophilic and aromatic residues of TM III, V, and VI (valine, leucine, phenylalanine, tyrosine). The allosteric binding pocket is formed by residues of the ECL2, TM V and VI and separated by $Arg265^{6.55}$ from the orthosteric binding site. At $P2Y_2R$, the AQ antagonist can reach the hydrophobic binding pocket, while at $P2Y_4R$, ring E is predicted to be prevented from reaching the hydrophobic binding site due to steric hindrance, and therefore to bind to an allosteric pocket.

predicted to project towards the aromatic binding pocket where the sulfonate can form ionic interactions with $Arg265^{6.55}$.

RB-2 as well as its smaller derivatives showed significant decreases in potency at the $F200^{5.38}Y$-$P2Y_4R$ mutant (3- to > 200-fold). Phe200 is located deep in the aromatic binding pocket where ring E of small AQ derivatives and sulfonate-substituted ring F of RB-2 may bind. The introduction of a hydroxy group in the binding pocket in the case of the $F200^{5.38}Y$ mutant limits the available space and increases the ratio of hydrophilic, solvent-accessible surface area. This is consistent with the proposed docking studies, as the investigated smaller AQ derivatives possess lipophilic substituents at ring E which benefit from hydrophobic interactions with $Phe200^{5.38}$. The potency of PSB-1699 (**12**), which contains a longer linker, was most strongly decreased (> 200-fold, IC_{50} > 10 μM) at the $F200^{5.38}Y$ mutant, since the pyridylmethylthio group may bind deeper in the aromatic binding pocket, thus forming π-π-interactions. Space limitations by the hydroxy group of the $F200^{5.38}Y$ mutant therefore resulted in a much larger decrease in the potency of PSB-1699 as compared to the other AQ derivatives. The mutation of $Tyr197^{5.35}$ to alanine had no negative impact on the potencies of the investigated antagonists. Therefore, we assume that no strong π–π-interactions between $Tyr197^{5.35}$ and aromatic rings of the AQ core structure are formed, which is consistent with our proposed docking position. The $Y197^{5.35}F$ mutation led to a decrease of potency of RB-2 (**6**), PSB-16133 (**10**), PSB-16135 (**11**) and PSB-1699 (**12**) (4-, 3- to 6-fold). Therefore, hydrogen bond interactions between the hydroxy group of $Tyr197^{5.35}$ and the linker between ring D and E are feasible. The results indicated that the larger RB-2 interacts similarly as the smaller AQ derivatives **9–11** with the $P2Y_4R$, while it likely has a different binding mode at $P2Y_2R$.

Again, PSB-1699 (**12**) shows a different profile than the other AQ derivatives. Here, $R190^{ECL2}A$ and $D195^{5.33}A$ mutation led to a complete loss of potency. The main difference between PSB-1699 and the other investigated AQ antagonists is a longer linker connecting the thioether with ring E, resulting in higher flexibility and at the same time requiring more space in the binding site. Therefore, changes in the flexibility of the ECL2 could greatly affect the potency of PSB-1699. As mentioned above, $Arg190^{ECL2}$ is possibly involved in an ionic lock close to the extracellular space modulating the flexibility of the ECL2. Although only the mutation of $Arg190^{ECL2}$ but not that of $Asp195^{5.33}$ affected the potency of agonists, it is possible that $Asp195^{5.33}$ affects antagonist potency through interactions with other residues by modulating the flexibility of the ECL2. These results, in addition to those described for the $Y197^{5.35}A/F$ and $F200^{5.38}A/Y$ mutants, indicate that PSB-1699 may bind closer to the aromatic binding site based on its longer linker. The orthosteric or allosteric binding mode of small AQ derivatives at $P2Y_2$- and $P2Y_4Rs$ may thereby be determined by the structure of ring D and E. Ring E of AQ derivatives can be accommodated in the larger orthosteric site of $P2Y_2R$, whereas space restrictions likely by a rotamer of $Arg265^{6.55}$ impede the access to the orthosteric binding site of $P2Y_4R$. Increased flexibility of ring E (in PSB-1699) may allow interactions with amino acid residues close to the orthosteric binding site since the molecule can adapt to the steric constraints.

To confirm the binding mode of PSB-1699 in the $P2Y_4R$ ligand pocket, the mechanism of inhibition was determined by Schild analysis using calcium mobilization assays. With increasing concentrations, competitive antagonists are expected to display a parallel rightward shift of the concentration–response curve of an agonist. In contrast, allosteric, noncompetitive antagonists will decrease the maximal effect of the agonist with or without a significant rightward shift [32,47,61]. Our data suggests PSB-1699 may be an allosteric (non-competitive) inhibitor of hP2Y$_4$R activation by UTP as increasing concentrations of the antagonist (0.500–50.0 μM) significantly decreased the maximal effect of UTP at the wt hP2Y$_4$R (from 100 ± 4% to 34 ± 4%) showing little to no significant change in its EC_{50} value (Fig. 20; see Supplementary Table S6 for EC_{50} values).

3.5.4.2. AR-C118925. Large decreases in potency of the antagonist AR-C118925 (**7**), which is moderately potent at $P2Y_4R$ (IC_{50} 5730 ± 821 nM), were observed at the $N170^{4.60}V$, $D195^{5.33}S$ and $F200^{5.38}Y$ mutants (> 15-fold, IC_{50} > 10 μM) of $P2Y_4R$, minor changes resulted from the $R190^{ECL2}A$, $E193^{ECL2}A$, $Y197^{5.35}F$, and $F200^{5.38}A$ mutations. An increase in potency was seen for the $D195^{5.33}A$ and $Y197^{5.35}A$ mutants (3- to 4-fold). $Asn170^{4.60}$ is placed in TM IV very close to the nucleotide binding pocket. The homology model and docking results suggest that hydrogen bonds may be formed with $Tyr116^{3.33}$, leading to the assumption that $Asn170^{4.60}$ is involved in regulation of the aromatic network. Increases in space in the binding pocket through mutation of $Tyr197^{5.35}$ or $Phe200^{5.38}$ to alanine had no negative impact on the potency of AR-C118925. The substitution with the respective other aromatic amino acid ($Y197^{5.35}F$, $F200^{5.38}Y$) led to a 2-fold (IC_{50} 9790 ± 884 nM) and > 20-fold (IC_{50} > 10 μM) decrease in potency, respectively, indicating that hydrogen bonds affected the binding of AR-C118925 to the $P2Y_4R$. $Tyr197^{5.35}$ and $Phe200^{5.38}$ may modulate the flexibility of the ECL2, which could also explain the effects of charged amino acids present in the ECL2 ($Arg190^{ECL2}$, $Glu193^{ECL2}$, $Asp195^{5.33}$) on the potency of AR-C118925. The selectivity of AR-C118925 for $P2Y_2R$ versus $P2Y_4R$ may be explained through increased lipophilicity or favorable aromatic stacking in the binding cavity for the dibenzocycloheptenyl moiety, as $Asn170^{4.60}$ of $P2Y_4R$ is replaced by a valine, and $Tyr197^{5.35}$ by phenylalanine in $P2Y_2R$.

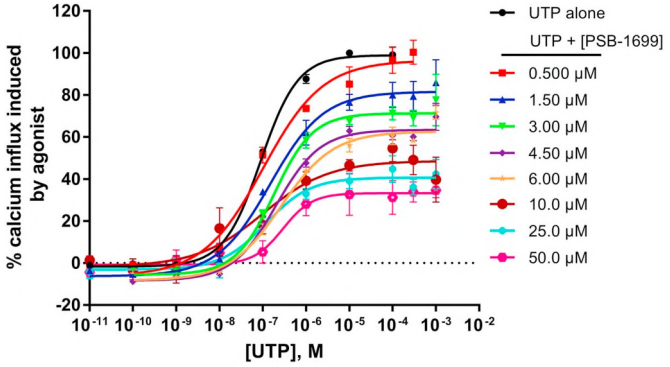

Fig. 20. Concentration–response curves of UTP at the wt *h*P2Y$_4$R after pre-incubation with fixed concentrations of PSB-1699 determined using the calcium mobilization assay. The receptor was stably expressed in 1321 N1 astrocytoma cells. Each data point represents mean ± SEM of 3–4 independent determinations each in duplicates. In the presence of increasing concentrations of PSB-1699, the maximal effect of UTP was decreased whereas the EC_{50} values were hardly affected (one-way ANOVA with Dunnett's post-hoc test). The EC_{50} values and maximum effects of UTP are shown in Supporting Information Table S6.

4. Conclusions

Docking and mutagenesis results suggest a binding mode of agonists at P2Y$_2$- and P2Y$_4$R comparable to that of agonists in the crystal structure of *h*P2Y$_{12}$R [52], where the phosphate groups interact with negatively charged residues, and a lipophilic binding pocket accommodates the nucleobase. The putative agonist binding mode of P2Y$_2$- and P2Y$_4$R differs from the one observed in the crystal structure of *h*P2Y$_1$R in complex with the nucleotide antagonist MRS2500 (**13**) [49]. The agonists UTP (**1**) and ATP (**2**) contain a 5′-triphosphate chain, while the P2Y$_1$R antagonist MRS2500 (**13**) of the crystal structure bears single phosphate groups in the 3′- and 5′-position of the ribose moiety, which is the probable reason for different binding modes. We were able to elucidate the role of Asp185^{ECL2} of P2Y$_2$R, which likely forms an ionic lock with an arginine in TM VII. UTP and ATP share a common pharmacological profile of full agonists at P2Y$_2$R, while Ap$_4$A (**3**) and MRS4062 (**5**) acting as partial agonists, appear to induce a different active receptor conformer. Phe113$^{3.32}$ and Asp185^{ECL2} play a key role in receptor activation by Ap$_4$A and MRS4062, since mutation of both amino acid residues resulted in a complete loss of receptor activation by agonists 3 and 5, in contrast to UTP and ATP. The charged residues Arg190^{ECL2}, Glu193^{ECL2} and Asp195$^{5.33}$, predicted to be distant from the putative ligand binding site of P2Y$_4$R, affected the potency of agonists and antagonists when mutated to alanine, which is consistent with previous observations for *h*P2Y$_2$R. Ligand recognition is therefore not only limited to the orthosteric binding site but can also be altered through interactions between residues close to the ECL2, which may affect loop flexibility. The binding mode of both, agonists and antagonists, may be determined through an aromatic network consisting of residues of TM III, V and VI. The P2Y$_2$R may be privileged to accept ATP and other adenine nucleotide-derived agonists due to a more spacious nucleobase binding cavity, as the increase in space in the orthosteric binding site of the P2Y$_4$R-Y197$^{5.35}$A mutant resulted in reintroduction of ATP-sensitivity.

The investigated AQ antagonists share a similar binding cavity for the AQ core, whereas substituents (rings D and E) of PSB-1699, PSB-16133 and PSB-16135 project towards an allosteric binding domain in P2Y$_4$R. The antagonist PSB-1699 appears to form additional interactions with aromatic residues of P2Y$_4$R (Phe200$^{5.38}$), and with aromatic residues close to the putative orthosteric binding site (Phe113$^{3.32}$) and close to the ECL2 (Phe195$^{5.35}$) of P2Y$_2$R due to its longer linker in comparison to the other investigated AQ derivatives. The binding modes of smaller AQ derivatives at P2Y$_2$- and P2Y$_4$Rs might therefore be dependent on the structure and flexibility of ring E, as well as the available space in the binding cavities resulting in either orthosteric or allosteric binding.

The antagonist AR-C118925 likely binds to the orthosteric site of both receptor subtypes. The ECL2 possibly plays a key role in binding of AR-C118925 in the case of P2Y$_4$R while no similar observation has been made for the investigated mutants of P2Y$_2$R. The selectivity for P2Y$_2$R could be explained by increased lipophilicity in the binding pocket resulting in tighter binding and stronger π–π-stacking.

Altogether, the data from the current work provides further insights into the architecture of ligand–receptor interactions and ligand selectivity of P2Y$_2$- and P2Y$_4$Rs. Docking studies at homology models predicted key residues with direct ligand interactions and those remote to the orthosteric binding site for developing novel therapeutics. These findings, supported by mutagenesis and pharmacological studies, and the refined homology models will aid future rational structure-based ligand design for P2Y$_2$- and P2Y$_4$Rs for both of which potent and selective ligands are badly needed to perform target validation studies.

Declaration of Competing Interests

The authors declare that they have no known competing financial interests or personal relationships that could have appeared to influence the work reported in this paper.

Acknowledgements

This study was supported by the German Research Foundation (DFG, Research Training group GRK 1873) and by the Federal Ministry of Education and Research (BMBF, project BIGS DrugS). I.A. obtained a PhD scholarship by the Deutscher Akademischer Austauschdienst (DAAD). Y.B. is grateful for an SQU grant (SR/SCI/CHEM/15/01).

Appendix A. Supplementary data

Supplementary material.

References

[1] G. Burnstock, M. Williams, P2 purinergic receptors: modulation of cell function and therapeutic potential, J. Pharmacol. Exp. Ther. 295 (2000) 862–869.
[2] A. Brunschweiger, C.E. Müller, P2 receptors activated by uracil nucleotides-an update, Curr. Med. Chem. 13 (2006) 289–312.
[3] K.A. Jacobson, C.E. Müller, Medicinal chemistry of adenosine, P2Y and P2X receptors, Neuropharmacology 104 (2016) 31–49.
[4] G. Burnstock, Purinergic receptors, J. Theor. Biol. 62 (1976) 491–503.
[5] K.A. Jacobson, J.M. Boeynaems, P2Y nucleotide receptors: promise of therapeutic applications, Drug Discov. Today 15 (2010) 570–578.
[6] P. Savi, J.M. Herbert, Clopidogrel and ticlopidine: P2Y$_{12}$ adenosine diphosphate-receptor antagonists for the prevention of atherothrombosis, Semin. Thromb. Hemost. 31 (2005) 174–183.
[7] D.J. Angiolillo, J.L. Ferreiro, Platelet adenosine diphosphate P2Y$_{12}$ receptor antagonism: benefits and limitations of current treatment strategies and future directions, Rev. Esp. Cardiol. 63 (2010) 60–76.
[8] Y. Baqi, C.E. Müller, Antithrombotic P2Y$_{12}$ receptor antagonists: recent developments in drug discovery, Drug Discov. Today 6446 (2018).
[9] M. Rafehi, C.E. Müller, Tools and drugs for uracil nucleotide-activated P2Y receptors, Pharmacol. Ther. 190 (2018) 24–80.
[10] G.P. Connolly, P.J. Harrison, T.W. Stone, Action of purine and pyrimidine nucleotides on the rat superior cervical ganglion, Br. J. Pharmacol. 110 (1993) 1297–1304.
[11] G.P. Connolly, N.J. Abbott, C. Demaine, J.A. Duley, Investigation of receptors responsive to pyrimidines, Trends Pharmacol. Sci. 18 (1997) 413–414.
[12] P. Hillmann, G.Y. Ko, A. Spinrath, A. Raulf, I. von Kügelgen, S.C. Wolff, R.A. Nicholas, E. Kostenis, H.D. Höltje, C.E. Müller, Key determinants of nucleotide-activated G protein-coupled P2Y$_2$ receptor function revealed by chemical and pharmacological experiments, mutagenesis and homology modeling, J. Med. Chem. 52 (2009) 2762–2775.
[13] J. Pintor, A. Peral, C.H.V. Hoyle, C. Redick, J. Douglass, I. Sims, B. Yerxa, Effects of diadenosine polyphosphates on tear secretion in new zealand white rabbits, J. Pharmacol. Exp. Ther. 300 (2002) 291–297.
[14] D.J. Moore, J.K. Chambers, J.P. Wahlin, K.B. Tan, G.B. Moore, O. Jenkins, P.C. Emson, P.R. Murdock, Expression pattern of human P2Y receptor subtypes: a quantitative reverse transcription-polymerase chain reaction study, Biochim. Biophys. Acta 1521 (2001) 107–119.
[15] A.M. Wong, A.W. Chow, S.C. Au, C.C. Wong, W.H. Ko, Apical versus basolateral P2Y$_6$ receptor-mediated Cl^- secretion in immortalized bronchial epithelia, Am. J.

Respir. Cell Mol. Biol. 40 (2009) 733–745.
[16] J.B. Regard, I.T. Sato, S.R. Coughlin, Anatomical profiling of G protein-coupled receptor expression, Cell 135 (2009) 561–571.
[17] M. León-Otegui, R. Gómez-Villafuertes, J.I. Díaz-Hernández, M. Díaz-Hernández, M.T. Miras-Portugal, J. Gualix, Opposite effects of P2X7 and $P2Y_2$ nucleotide receptors on α-secretase-dependent APP processing in Neuro-2a cells, FEBS Lett. 585 (2011) 2255–2262.
[18] B.R. Yerxa, J.R. Sabater, C.W. Davis, M.J. Stutts, M. Picher, A.C. Jones, M. Cowlen, Pharmacology of INS37217 [P^1-(uridine 5′)-P^4-(2′-deoxycytidine 5′) tetraphosphate, tetrasodium salt], a next-generation $P2Y_2$ receptor agonist for the treatment of cystic fibrosis, J. Pharmacol. Exp. Ther. 302 (2002) 871–880.
[19] K.K. Nichols, B. Yerxa, D.J. Kellerman, Diquafosol tetrasodium: a novel dry eye therapy, Expert Opin. Investig. Drugs 13 (2004) 47–54.
[20] R. Deterding, G. Retsch-Bogart, L. Milgram, R. Gibson, C. Daines, P.L. Zeitlin, C. Milla, B. Marshall, L. LaVange, J. Engels, D. Mathews, J. Gorden, A. Schaberg, J. Williams, B. Ramsey, Safety and tolerability of denufosol tetrasodium inhalation solution, a novel $P2Y_2$ receptor agonist: results of a phase 1/phase 2 multicenter study in mild to moderate cystic fibrosis, Pediatr. Pulmonol. 39 (2005) 339–348.
[21] G.M. Keating, Diquafosol ophthalmic solution 3%: a review of its use in dry eye, Drugs 75 (2015) 911–922.
[22] R.B. Moss, Pitfalls of drug development: lessons learned from trials of denufosol in cystic fibrosis, J. Pediatr. 162 (2013) 676–680.
[23] L. Erb, C. Cao, D. Ajit, G.A. Weisman, P2Y receptors in Alzheimer's disease, Biol. Cell. 107 (2015) 1–21.
[24] E. Hochhauser, R. Cohen, M. Waldman, A. Maksin, A. Isak, D. Aravot, P.S. Jayasekara, C.E. Müller, K.A. Jacobson, A. Shainberg, $P2Y_2$ receptor agonist with enhanced stability protects the heart from ischemic damage in vitro and in vivo, Purinergic Signal 9 (2013) 633–642.
[25] R. Cohen, A. Shainberg, E. Hochhauser, Y. Cheporko, A. Tobar, E. Birk, L. Pinhas, J. Leipziger, J. Don, E. Porat, UTP reduces infarct size and improves mice heart function after myocardial infarct via $P2Y_2$ receptor, Biochem. Pharmacol. 82 (9) (2011) 1126–1133.
[26] D. Schumacher, B. Strilic, K.K. Sivaraj, N. Wettschureck, S. Offermanns, Platelet-derived nucleotides promote tumor-cell transendothelial migration and metastasis via $P2Y_2$ receptor, Cancer Cell 24 (2013) 130–137.
[27] D. Ajit, L.T. Woods, J.M. Camden, C.N. Thebeau, F.G. El-Sayed, G.W. Greeson, L. Erb, M.J. Petris, D.C. Miller, G.Y. Sun, G.A. Weisman, Loss of $P2Y_2$ nucleotide receptors enhances early pathology in the TgCRND8 mouse model of Alzheimer's disease, Mol. Neurobiol. 49 (2014) 1031–1042.
[28] C. Séror, M.-T. Melki, F. Subra, S.Q. Raza, M. Bras, H. Saïdi, R. Nardacci, L. Voisin, A. Paoletti, F. Law, I. Martins, A. Amendola, A.A. Abdul-Sater, F. Ciccosanti, O. Delelis, F. Niedergang, S. Thierry, N. Said-Sadier, C. Lamaze, D. Métivier, J. Estaquier, G.M. Fimia, L. Falasca, R. Casetti, N. Modjtahedi, J. Kanellopoulos, J.-F. Mouscadet, D.M. Ojcius, M. Piacentini, M.-L. Gougeon, G. Kroemer, J.-L. Perfettini, Extracellular ATP acts on $P2Y_2$ purinergic receptors to facilitate HIV-1 infection, J. Exp. Med. 208 (2011) 1823–1834.
[29] S.A. Potthoff, J. Stegbauer, J. Becker, P.J. Wagenhaeuser, B. Duvnjak, L.C. Rump, O. Vonend, $P2Y_2$ receptor deficiency aggravates chronic kidney disease progression, Front. Physiol. 4 (2013) 1–9.
[30] B.K. Kishore, N.G. Carlson, C.M. Ecelbarger, D.E. Kohan, C.E. Müller, R.D. Nelson, J. Peti-Peterdi, Y. Zhang, Targeting renal purinergic signalling for the treatment of lithium-induced nephrogenic diabetes insipidus, Acta Physiol. 214 (2015) 176–188.
[31] J. Merz, P. Albrecht, S. von Garlen, I. Ahmed, D. Dimanski, D. Wolf, I. Hilgendorf, C. Härdtner, K. Grotius, F. Willecke, T. Heidt, H. Bugger, N. Hoppe, U. Kintscher, C. von zur Mühlen, M. Idzko, C. Bode, A. Zirlik, P. Stachon, Purinergic receptor Y2 ($P2Y_2$)-dependent VCAM-1 expression promotes immune cell infiltration in metabolic syndrome, Basic Res. Cardiol. 113 (2018) 45.
[32] M. Rafehi, J.C. Burbiel, I.Y. Attah, A. Abdelrahman, C.E. Müller, Synthesis, characterization, and in vitro evaluation of the selective $P2Y_2$ receptor antagonist AR-C118925, Purinergic Signal 13 (2016) 89–103.
[33] P.A. Kemp, R.A. Sugar, A.D. Jackson, Nucleotide-mediated mucin secretion from differentiated human bronchial epithelial cells, Am. J. Respir. Cell Mol. Biol. 31 (2004) 446–455.
[34] N. Kindon, A. Davis, I. Dougall, J. Dixon, T. Johnson, I. Walters, S. Thom, K. McKechnie, P. Meghani, M.J. Stocks, From utp to ar-c118925, the discovery of a potent non nucleotide antagonist of the p2y2receptor, Bioorganic Med. Chem. Lett. 27 (2017) 4849–4853.
[35] J.E. Matos, B. Robaye, J.M. Boeynaems, R. Beauwens, J. Leipziger, K^+ secretion activated by luminal $P2Y_2$ and $P2Y_4$ receptors in mouse colon, J. Physiol. 564 (2005) 269–279.
[36] E. Ghanem, B. Robaye, T. Leal, J. Leipziger, W. Van Driessche, R. Beauwens, J.-M. Boeynaems, The role of epithelial $P2Y_2$ and $P2Y_4$ receptors in the regulation of intestinal chloride secretion, Br. J. Pharmacol. 146 (2005) 364–369.
[37] M.M. Ward, T. Puthussery, E.L. Fletcher, Localization and possible function of $P2Y_4$ receptors in the rodent retina, Neuroscience 155 (2008) 1262–1274.
[38] M.D. Tran, P2 receptor stimulation induces amyloid precursor protein production and secretion in rat cortical astrocytes, Neurosci. Lett. 492 (2011) 155–159.
[39] B. Robaye, E. Ghanem, F. Wilkin, D. Fokan, W. Van Driessche, S. Schurmans, J.-M. Boeynaems, R. Beauwens, Loss of nucleotide regulation of epithelial chloride transport in the jejunum of $P2Y_4$-null mice, Mol. Pharmacol. 63 (2003) 777–783.
[40] H. Li, C. Chen, Y. Dou, H. Wu, Y. Liu, H.-F. Lou, J. Zhang, X. Li, H. Wang, S. Duan, $P2Y_4$ receptor-mediated pinocytosis contributes to amyloid beta-induced self-uptake by microglia, Mol. Cell. Biol. 33 (2013) 4282–4293.
[41] F. Cavaliere, S. Amadio, D.F. Angelini, G. Sancesario, G. Bernardi, C. Volonté, Role of the metabotropic $P2Y_4$ receptor during hypoglycemia: cross talk with the ionotropic NMDAR1 receptor, Exp. Cell Res. 300 (2004) 149–158.
[42] M. Horckmans, H. Esfahani, C. Beauloye, S. Clouet, L. di Pietrantonio, B. Robaye, J.-L. Balligand, J.-M. Boeynaems, C. Dessy, D. Communi, Loss of Mouse $P2Y_4$ nucleotide receptor protects against myocardial infarction through endothelin-1 downregulation, J. Immunol. 194 (2015) 1874–1881.
[43] A. Lemaire, M. Vanorlé, M. Horckmans, L. di Pietrantonio, S. Clouet, B. Robaye, J.-M. Boeynaems, D. Communi, Mouse $P2Y_4$ nucleotide receptor is a negative regulator of cardiac adipose-derived stem cell differentiation and cardiac fat formation, Stem Cells Dev. 26 (2017) 363–373.
[44] H. Maruoka, M.P.S. Jayasekara, M.O. Barrett, D.A. Franklin, S. De Castro, N. Kim, S. Costanzi, T.K. Harden, K.A. Jacobson, Pyrimidine nucleotides with 4-alkyloxyimino and terminal tetraphosphate δ-ester modifications as selective agonists of the $P2Y_4$ receptor, J. Med. Chem. 54 (2011) 4018–4033.
[45] G. Lambrecht, K. Braun, M. Damer, M. Ganso, C. Hildebrandt, H. Ullmann, M.U. Kassack, P. Nickel, Structure-activity relationships of suramin and pyridoxal-5′-phosphate derivatives as P2 receptor antagonists, Curr. Pharm. Des. 8 (2002) 2371–2399.
[46] I. von Kügelgen, K. Hoffmann, Pharmacology and structure of P2Y receptors, Neuropharmacology 104 (2016) 50–61.
[47] M. Rafehi, E.M. Malik, A. Neumann, A. Abdelrahman, T. Hanck, V. Namasivayam, C.E. Müller, Y. Baqi, Development of potent and selective antagonists for the UTP-activated $P2Y_4$ receptor, J. Med. Chem. 60 (2017) 3020–3038.
[48] K. Zhang, J. Zhang, Z.-G. Gao, D. Zhang, L. Zhu, G.W. Han, S.M. Moss, S. Paoletta, E. Kiselev, W. Lu, G. Fenalti, W. Zhang, C.E. Müller, H. Yang, H. Jiang, V. Cherezov, V. Katritch, K.A. Jacobson, R.C. Stevens, B. Wu, Q. Zhao, Structure of the human $P2Y_{12}$ receptor in complex with an antithrombotic drug, Nature 509 (2014) 115–118.
[49] D. Zhang, Z.-G. Gao, K. Zhang, E. Kiselev, S. Crane, J. Wang, S. Paoletta, C. Yi, L. Ma, W. Zhang, G.W. Han, H. Liu, V. Cherezov, V. Katritch, H. Jiang, R.C. Stevens, K.A. Jacobson, Q. Zhao, B. Wu, Two disparate ligand-binding sites in the human $P2Y_1$ receptor, Nature 520 (2015) 317–321.
[50] M. Rafehi, A. Neumann, Y. Baqi, E.M. Malik, M. Wiese, V. Namasivayam, C.E. Müller, Molecular recognition of agonists and antagonists by the nucleotide-activated G protein-coupled $P2Y_2$ receptor, J. Med. Chem. 60 (2017) 8425–8440.
[51] B. Webb, A. Sali, Protein structure modeling with modeller, Humana Press, New York, NY, 2017, pp. 39–54.
[52] J. Zhang, K. Zhang, Z.-G. Gao, S. Paoletta, D. Zhang, G.W. Han, T. Li, L. Ma, W. Zhang, C.E. Müller, H. Yang, H. Jiang, V. Cherezov, V. Katritch, K.A. Jacobson, R.C. Stevens, B. Wu, Q. Zhao, Agonist-bound structure of the human $P2Y_{12}$ receptor, Nature 509 (2014) 119–122.
[53] A. Bateman, M.J. Martin, C. O'Donovan, M. Magrane, E. Alpi, R. Antunes, B. Bely, M. Bingley, C. Bonilla, R. Britto, B. Bursteinas, H. Bye-AJee, A. Cowley, A. Da Silva, M. De Giorgi, T. Dogan, F. Fazzini, L.G. Castro, L. Figueira, P. Garmiri, G. Georghiou, D. Gonzalez, E. Hatton-Ellis, W. Li, W. Liu, R. Lopez, J. Luo, Y. Lussi, A. MacDougall, A. Nightingale, B. Palka, K. Pichler, D. Poggioli, S. Pundir, L. Pureza, G. Qi, S. Rosanoff, R. Saidi, T. Sawford, A. Shypitsyna, E. Speretta, E. Turner, N. Tyagi, V. Volynkin, T. Wardell, K. Warner, X. Watkins, R. Zaru, H. Zellner, I. Xenarios, L. Bougueleret, A. Bridge, S. Poux, N. Redaschi, L. Aimo, G. ArgoudPuy, A. Auchincloss, K. Axelsen, P. Bansal, D. Baratin, M.C. Blatter, B. Boeckmann, J. Bolleman, E. Boutet, L. Breuza, C. Casal-Casas, E. De Castro, E. Coudert, B. Cuche, M. Doche, D. Dornevil, S. Duvaud, A. Estreicher, L. Famiglietti, M. Feuermann, E. Gasteiger, S. Gehant, V. Gerritsen, A. Gos, N. Gruaz-Gumowski, U. Hinz, C. Hulo, F. Jungo, G. Keller, V. Lara, P. Lemercier, D. Lieberherr, T. Lombardot, X. Martin, P. Masson, A. Morgat, T. Neto, N. Nouspikel, S. Paesano, I. Pedruzzi, S. Pilbout, M. Pozzato, M. Pruess, C. Rivoire, B. Roechert, M. Schneider, C. Sigrist, K. Sonesson, S. Staehli, A. Stutz, S. Sundaram, M. Tognolli, L. Verbregue, A.L. Veuthey, C.H. Wu, C.N. Arighi, L. Arminski, C. Chen, Y. Chen, J.S. Garavelli, H. Huang, K. Laiho, P. McGarvey, D.A. Natale, K. Ross, C.R. Vinayaka, Q. Wang, Y. Wang, L.S. Yeh, J. Zhang, UniProt: the universal protein knowledgebase, Nucleic Acids Res. 45 (2017) D158–D169.
[54] L. Erb, R. Garrad, Y. Wang, T. Quinn, J.T. Turner, G.A. Weisman, Site-directed mutagenesis of P2U purinoceptors: positively charged amino acids in transmembrane helices 6 and 7 affect agonist potency and specificity, J. Biol. Chem. (1995) 4185–4188.
[55] C.L. Herold, A.D. Qi, T.K. Harden, R.A. Nicholas, Agonist versus antagonist action of ATP at the $P2Y_4$ receptor is determined by the second extracellular loop, J. Biol. Chem. 279 (2004) 11456–11464.
[56] P.J. Conn, A. Christopoulos, C.W. Lindsley, Allosteric modulators of GPCRs: a novel approach for the treatment of CNS disorders, Nat. Rev. Drug Discov. 8 (2009) 41–54.
[57] S. Yuan, H.C.S. Chan, H. Vogel, S. Filipek, R.C. Stevens, K. Palczewski, The molecular mechanism of $P2Y_1$ receptor activation, Angew. Chemie Int. Ed. 55 (2016) 10331–10335.
[58] C. Hoffmann, S. Moro, R.A. Nicholas, T.K. Harden, K.A. Jacobson, C. Hill, N. Carolina, The role of amino acids in extracellular loops of the human $P2Y_1$ receptor in surface expression and activation processes, J. Biol. Chem. 274 (1999) 14639–14647.
[59] T. Kenakin, Differences between natural and recombinant G-protein-coupled receptor systems with varying receptor G-protein stoichiometry, Trends Pharmacol. Sci. 18 (1997) 456–464.
[60] T.L. Kinzer-Ursem, J.J. Linderman, Both ligand- and cell-specific parameters control ligand agonism in a kinetic model of G protein-coupled receptor signaling, PLoS Comput. Biol. 3 (2007) 0084–0094.
[61] T. Kenakin, S. Jenkinson, C. Watson, Determining the potency and molecular mechanism of action of insurmountable antagonists, J. Pharmacol. Exp. Ther. 319 (2006) 710–723.